

Isotropic Activation Functions Enable Deindividuated Neurons and Adaptive Topologies

George Bird

Department of Computer Science
University of Manchester, UK
george.bird@postgrad.manchester.ac.uk

Abstract

Introduced is a methodology for adapting the topology of dense neural networks, enabled by isotropic activation functions. Achieved through prescribed reparameterisation symmetries and singular-value decomposition of affine maps, this diagonalises layers into one-to-one, ordered connections. This makes it simpler to assess the impact of individual connections on the function. Low-impact neurons can be removed (neurodegeneration), and a thresholded buffer of largely inactive ‘scaffold’ neurons is maintained (neurogenesis). These symmetry-led diagonalisation and structural changes are function-invariant, demonstrated to be computationally identical during neurogenesis, arbitrarily well approximated during neurodegeneration, and enable asymptotic 50% parameter sparsification of dense networks with identically preserved function. Thus, real-time restructuring of the architecture in response to task demands, task appending, removal or changes is shown. The approach is conceptually centred on primitive symmetry-prescriptions, through which isotropic functions are derived that feature explicit basis independence and a loss in the individuation of neurons implicit in typical elementwise functional forms. Hence, this allows freedom in the basis to which layers are decomposed and interpreted as individual artificial neurons, directly enabling this adaptive topology approach. Additionally, a new tunable model parameter, the ‘intrinsic length’, is introduced to improve this analytical invariance, alongside a generalised isotropic-perceptron architecture that enables parallel precomputation of all matrix-vector products and displays a nested functional class. Diagonalisation is suggested to offer new possibilities for interpretability and monitoring of isotropic networks.

1 Introduction

Neural plasticity in the quantity and connectivity of neurons is biologically advantageous [1–3] and routinely occurs in the development of the mammalian brain [4–7]. Shown to improve neural efficiency through controlled pruning [8, 9], with a benefit to initial overabundance [9], whilst enabling the accumulation of knowledge [3, 7], improving robustness [10] and function through growth [11, 7]. Hence, it is hypothesised that analogous behaviour within artificial neural networks will be similarly beneficial. The practical consequences of a network that can reliably adapt its architecture and connectivity in a real-time controlled manner may be transformative — and this constitutes a broad goal of architecture-based continual learning approaches [12].

Contemporary primitives, e.g. activation functions, many initialisations, normalisers, optimisers, and more, are typically constructed using elementwise functional forms. Historically, forms were inspired by biological neural systems [13]: “[...] *the conformity of their relations to those of the logic of propositions, insure that the relations of psychons are those of the two-valued logic of propositions*”, an initial framing helping to naturalise the eventual pervasive implementation of activation vectors being decomposed in a basis-dependent manner, interpreted as individual artificial ‘neuron’-like units

composed with scalar operations. Modern elementwise formulae apply univariate maps independently to components; a construction generalising from this original individuated neuron-derived premise.

Due to this individuated construction, architectural adaptation that closely preserves function is made difficult by densely interconnected networks, especially for neurodegeneration. This is one reason individual-connectivity pruning [14–17], rather than whole-neuron removal [18, 19], is often typical.

This ‘individuation’ limitation is inherent to most contemporary primitives, with few exceptions. Particularly those that can be classified by their equivalence class under reparameterisation [20, 21], which typically admit permutation-structured groups, e.g., permutation, hyperoctahedral, scaled-permutations, etc. [22]. It is posited that generalising primitive construction instead through a *broader symmetry-prescribed* approach is beneficial; exploring this allows novel admissible functional forms and new behaviours via intentionally introduced reparameterisation invariances. These symmetry-prescribed primitive reformulations are central to the introduced adaptive topology approach, which replaces the typical, derived, permutation symmetry with prescribed alternatives.

Basis-independent formulations can then be achieved by replacing discrete symmetries with continuous ones. Namely, continuous orthogonal equivariance symmetry is used as a foundation for activation functions. This choice of continuous group prescription still permits non-linear functions on the magnitude, making it well-suited for activation functions, whilst the orthogonal group is also a supergroup of the permutation group, $O(n) \supset S_n$, offering a minimal, natural generalisation for reformulation. *Emergent* from this symmetry redefinition is a more generalised concept of neurons, which are ‘deindividuated’, since there is no function-distinguished basis for decomposition [23–25].

Enabled by this is a novel methodology for dynamic topologies, based on the observation that these orthogonal-(equivariant)-symmetry-derived reformulations, termed “isotropic primitives”, commute with orthogonal-group actions. Considering this in tandem with singular value decomposition (SVD), for dynamical networks, or independent component analysis (ICA) [26–28], for interpretable networks, which both yield standard orthogonal matrices able to commute with these isotropic functions by their symmetry-led design. Combining SVD’s properties thus enables a diagonalised topology by reparameterising the networks with its orthogonal matrices into a simpler one-to-one connectivity. This simplifies the complexity of full neurodegeneration by making it equivalent to connectivity pruning. Using an ICA representation derived from dataset activations may better represent a network for interpretability and real-time monitoring, up to ICA’s own concept resolvability.

This diagonalising reparameterisation procedure has *no functional degradation* analytically, owing to the primitive’s basis independence, and, in practice, only a negligible change due to machine precision and propagation thereof. Hence, equivalence classes are expanded to full architectural adaptations, not just static reparameterisations. These are exact for neurogenesis and closely approximate for neurodegeneration, beyond what is possible with classical parameter relabelling. The full adaptive-topology procedure introduced here incorporates this diagonalisation with thresholding to enable real-time adaptations in response to task demand. Due to its distinctive primitives, this approach bears limited similarity to prior adaptive network implementations; comparisons are discussed in *App. H*.

This procedure is unique to the continuous-symmetry prescribed primitives, indicating both the flexible use cases of these alternative isotropic formulations and a benefit of broader exploration of primitive symmetry prescription in *general* practice. The primary contributions are:

1. **Conceptual Contribution:** Functional forms are historically derived from individual neurons as fundamental units to compose. From these symmetries are *since deduced*. Instead, an ontological reversal: treating symmetry as fundamental and neurons as emergent, induced by group representations. Formalised in *Eqns. 1 to 3*, these taxonomise symmetry prescriptions that admit novel functional forms with generalised notions of neurons. Adopting symmetry-prescriptive foundations offers an expanded class of functional forms that underpin *neural* learning systems and are argued to be worth exploring more generally. This constitutes the broader objective that the adaptive architectures begin to pursue and evidence.
2. **Reformulation Contribution:** With this enriched design space, continuous-(orthogonal) symmetry-defined (isotropic) primitives are produced, displaying a crucial basis-independence absent in elementwise formulae, whilst implicitly generalising the neuron.
3. **Practical Contribution:** Leveraging this allows affine maps to be represented diagonally, and, with singular-value thresholding, enables dynamical architectures, alongside asymptotic 50% perfect sparsification, ICA-representations and parallelised matrix-vector products.

2 Theoretical Background

An overview of the symmetry-prescribed framework is provided, and it is then used to define isotropic activation functions that commute with orthogonal-group actions. Finally, layerwise diagonalisation and sparsification are detailed, culminating in the adaptive topology procedure. This is detailed for multilayer perceptrons, whilst *App D* presents a conceptual generalisation for convolution[29, 30].

2.1 Orthogonal Reformulations: Isotropic Activation Functions

Proposed is a prescriptive use of symmetry groups, \mathcal{G} , with their actions, $g \in \mathcal{G}$, acting on functions, f of a (potentially singleton) functional class \mathcal{F} in categorisable ways, such as through matrix representations $\mathbf{G} = \varrho(g)$. These are expressed through relations *Eqns. 1* \Rightarrow *2* \Rightarrow *3* — abridged from Bird [31]’s symmetry taxonomy. *Eqn. 2*’s probabilistic category is unnecessary for adaptive networks but provided for completeness, with intentionally flexible probability measure \mathbb{P} , e.g. for initialisers.

$$\forall g \in \mathcal{G}, \forall f \in \mathcal{F} : \varrho^{(1)}(g) \circ f \circ \varrho^{(2)}(g^{-1}) = f \quad (1)$$

$$\forall g \in \mathcal{G}, \forall f \in \mathcal{F} : \mathbb{P}\left(\varrho^{(1)}(g) \circ f \circ \varrho^{(2)}(g^{-1})\right) = \mathbb{P}(f) \quad (2)$$

$$\forall g \in \mathcal{G}, \forall f \in \mathcal{F} : \varrho^{(1)}(g) \circ f \circ \varrho^{(2)}(g^{-1}) \in \mathcal{F} \quad (3)$$

These detail three different ‘strength’ symmetry relations over the functional class, termed “algebraic”, “probabilistic” and “closure” for *Eqns. 1, 2* and *3*, respectively. These relations can serve as a foundation for activation functions, normalisers, initialisers, optimisers and further primitives for categorising through underlying symmetry properties. In isolation, these are *not* to be confused with reparameterisation invariances (parameter symmetries), which typically consist of pairings of one-sided closures often through algebraic intertwiners — a setup utilised in the subsequent section.

Defining isotropic functions as specifically algebraic-function constraints of standard representations of the orthogonal group family *maximally* (no supergroup), $\varrho : O(n) \rightarrow \text{GL}_n(\mathbb{R})$. These orthogonal matrices can be notated in shorthand as $\mathbf{R} \in O(n)$ for n width layers, and the algebraic constraint of *Eqn. 1* can then be simplified under these conditions to *Eqn. 4* for the function $\mathbf{f} : \mathbb{R}^n \rightarrow \mathbb{R}^n$.

$$\forall \mathbf{R} \in O(n), \forall \vec{x} \in \mathbb{R}^n : [\mathbf{R}, \mathbf{f}] = \mathbf{R} \circ \mathbf{f} - \mathbf{f} \circ \mathbf{R} = 0 \quad \text{equally} \quad \mathbf{f}(\mathbf{R}\vec{x}) = \mathbf{R}\mathbf{f}(\vec{x}) \quad (4)$$

These can be shown to be maximally satisfied by the general multivariate functional form shown in *Eqn. 5*, for a non-linear univariate function $\sigma(x)$. Any supergroup is also feasible for the subsequent diagonalisation, as it preserves this equivariance; however, the presence and nature of the respective non-linearity should be considered. The particular σ is otherwise unimportant for subsequent sections.

$$\mathbf{f}(\vec{x}) = \sigma(\|\vec{x}\|_2) \hat{x} \quad \text{or} \quad \mathbf{f}(\vec{x}) = \tilde{\sigma}(\|\vec{x}\|_2) \vec{x} \quad \text{or} \quad \mathbf{f}(\vec{x}) = \bar{\sigma}(\vec{x}^T \vec{x}) \vec{x} \quad (5)$$

Several placeholders may be suggested for σ , e.g. \tanh ; however, this superficially replicates existing activation functions, and there is no reason to assume any continued optimality in this altered form.

Adopting this ontology entails treating neuron individuation not as an intrinsic property of the vector space or network but as an induced artefact of the *chosen* group representations used to construct primitives under *Eqns. 1* through *3*. Matrix representations of the permutation group are generally not fixed under standard orthogonal, $\mathbf{R} \in O(n) \setminus P$, conjugation: $\{\varrho(\pi) | \pi \in S_n\} = P \neq \{\mathbf{R}\mathbf{P}_\pi\mathbf{R}^T | \mathbf{P}_\pi \in P\}$. Thus, constraining a functional form to be *maximally* equivariant to one such matrix representation introduces a *representation-specific* basis dependence in the admitted functional form. For a conjugated standard permutation representation, $\mathbf{R}\mathbf{P}_\pi\mathbf{R}^T$, this anisotropy distinguishes various vectors, particularly the unordered columns of \mathbf{R} , selecting an *absolute frame* in the function’s codomain. These distinguished columns of \mathbf{R} correspond to, and make special, the classical historical notion of artificial neurons. Such individuation ceases for orthogonal-prescribed isotropic functions: $\{\varrho'(Q) | Q \in O(n)\} = O = \{\mathbf{R}\mathbf{Q}\mathbf{R}^T | \mathbf{Q} \in O\}$, where no direction is inherently distinguished by the group representation’s admitted functional forms. Thus, group representations precede the individuated, characteristic [32, 33, 24] nature of emergent neurons. Broadening to deindividuated neurons is a crucial generalisation for this paper’s approach to adaptive architectures.

2.2 Layerwise Affine Diagonalisation

Full singular value decomposition (SVD) of \mathbf{A} produces $\mathbf{A} = \mathbf{R}\mathbf{\Lambda}\mathbf{Q}^T$, with diagonal $\mathbf{\Lambda} = \mathbf{\Lambda} \odot \mathbf{I}$, and orthogonal matrices $\mathbf{R}, \mathbf{Q} \in O(n)$, which can be used to transform an affine map, shown in *Eqn. 6*.

$$\mathbf{W}\vec{x} + \vec{b} = \mathbf{R}\mathbf{\Lambda}\mathbf{Q}^T\vec{x} + \vec{b} \quad (6)$$

Then, generalising this to performing the decomposition on the middle affine map of a three-layer perceptron and using the by-design orthogonal equivariance of isotropic functions enables an overall function-invariant reparameterisation. This is unusual in that it leverages this *continuous* symmetry definition across *three* layers, acting twice concurrently on both sides of the layer. With the choice of SVD, this forms a diagonalised representation of the middle layer (or *App. E*, an ICA representation).

For a multilayer perceptron (MLP), this minimally necessitates the orthogonal algebraic equivariance, by constraint of *Eqn. 1* on \mathbf{f} , alongside both standard and trivial orthogonal representations as single-sided closures on each sandwiching affine layer, described by *Eqn. 3* — satisfied by the existing $O(n) \subset GL_n(\mathbb{R})$ two-sided closure of affine maps, enabling the desired equivalence class without modification. One may also choose an initialiser with orthogonally symmetric distribution by *Eqn. 2*.

Reparameterisation for three such affine maps, f_{aff} and two, potentially differing, isotropic activation functions f_{iso} , is demonstrated in *Eqns. 7* through *11*. No assumptions need to be made about layer widths, which may vary layer-wise, given this procedure’s generality.

$$\mathbf{f} = f_{\text{Aff.3}} \circ f_{\text{Iso.2}} \circ f_{\text{Aff.2}} \circ f_{\text{Iso.1}} \circ f_{\text{Aff.1}} \quad (7)$$

$$\mathbf{f}(\vec{x}) = \mathbf{W}_3 f_{\text{Iso.2}} \left(\mathbf{W}_2 f_{\text{Iso.1}} \left(\mathbf{W}_1 \vec{x} + \vec{b}_1 \right) + \vec{b}_2 \right) + \vec{b}_3 \quad (8)$$

Then one can apply the SVD to the weight \mathbf{W}_2 whilst inserting an identity matrix, $\mathbf{I}_n = \mathbf{R}\mathbf{R}^T$.

$$\mathbf{f}(\vec{x}) = \mathbf{W}_3 f_{\text{Iso.2}} \left(\underbrace{(\mathbf{R}\mathbf{R}^T)}_{\mathbf{I}_n} \left(\mathbf{R}\mathbf{\Lambda}\mathbf{Q}^T f_{\text{Iso.1}} \left(\mathbf{W}_1 \vec{x} + \vec{b}_1 \right) + \vec{b}_2 \right) \right) + \vec{b}_3 \quad (9)$$

$$\mathbf{f}(\vec{x}) = \underbrace{\mathbf{W}_3 \mathbf{R}}_{\mathbf{W}'_3} f_{\text{Iso.2}} \left(\mathbf{\Lambda} f_{\text{Iso.1}} \left(\underbrace{\mathbf{Q}^T \mathbf{W}_1}_{\mathbf{W}'_1} \vec{x} + \underbrace{\mathbf{Q}^T \vec{b}_1}_{\vec{b}'_1} \right) + \underbrace{\mathbf{R}^T \vec{b}_2}_{\vec{b}'_2} \right) + \vec{b}_3 \quad (10)$$

Finally, reparameterising the affine layers with modified weights \mathbf{W}' and biases \vec{b}' .

$$\mathbf{f}(\vec{x}) = \mathbf{W}'_3 f_{\text{Iso.2}} \left(\mathbf{\Lambda} f_{\text{Iso.1}} \left(\mathbf{W}'_1 \vec{x} + \vec{b}'_1 \right) + \vec{b}'_2 \right) + \vec{b}_3 \quad (11)$$

$$\mathbf{f}(\vec{x}) = \mathbf{W}'_3 f_{\text{Iso.2}} \left(\vec{W} \odot f_{\text{Iso.1}} \left(\mathbf{W}'_1 \vec{x} + \vec{b}'_1 \right) + \vec{b}'_2 \right) + \vec{b}_3 \quad (12)$$

Hence, the central layer is diagonalised, whilst the MLP remains function-invariant overall to such a transformation. This layer is simplified to one-to-one connectivity, as depicted in *Fig. 1*. The singular values can be ordered, enabling a perturbative-like understanding of the layer’s simplified action — especially when incorporating normalisation or a magnitude-bounded \mathbf{f} . Similarly this can be expressed with a hadamard product, \odot , with parameterisation $\vec{W} = \text{diag}(\mathbf{\Lambda})$, as shown in *Eqn. 12*.

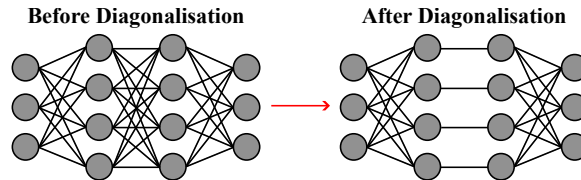


Figure 1: Illustrates the qualitative effects on a network undergoing full diagonalisation. The connectivity is simplified to a one-to-one correspondence between neurons on the chosen layer.

Practically, complete diagonalisation is not necessary for adaptive topologies or interpretability; instead, a left-sided partial diagonalisation, as shown in *Eqn. 13*, is sufficient and marginally more computationally efficient to enact. However, at inference time, full diagonalisation may provide substantial benefit by its significant sparsity whilst remaining analytically function-invariant.

$$\mathbf{f}(\vec{x}) = \mathbf{W}'_3 f_{\text{Iso.2}} \left(\mathbf{\Lambda} \mathbf{Q}^T f_{\text{Iso.1}} \left(\mathbf{W}_1 \vec{x} + \vec{b}_1 \right) + \vec{b}'_2 \right) + \vec{b}_3 \quad (13)$$

Finally, unlike traditional permutation reparameterisations, orthogonal transforms exhibit typical forward-pass function invariance but, novelly, display *variance* in their coupling to gradient-descent algorithms after transform — producing, sequentially backwards from the transform, a training-time-only breaking of the reparameterisation symmetry — absent at inference time. This optimiser connection may offer an insightful direction for future study, and is discussed in *App. A*.

2.2.1 Sparsification

A significant quality of isotropic activation functions in MLPs is this function-invariant SVD-based diagonalisation, as demonstrated. This feature is not limited to dynamic topology or interpretability considerations, but also to the considerable connectivity sparsity it affords.

Two directions may be taken for this, which may be performed just prior to inference time: Joint sparsity optimisation (JSO), which optimises over the multi-layer orthogonal direct-sum Lie group to minimise an objective function of parameter count via a continuous proxy — many such forms are applicable, including L_1 -norm-based approaches. Simpler still is an every-second layerwise diagonalisation, which asymptotically achieves an overall 50% parameter reduction, despite the model function being identical up to floating-point precision. For an odd-depth MLP, Eqn. 14, displays the sparsity factor, whilst Eqn. 15 is for the even depth case. Given $2D + 1$ and $2D$ affine layers respectively, each of N width, accounting to $(\dim \mathbf{W} + \dim \vec{b} = N^2 + N)$ parameters per layer.

$$S_{\text{odd}} = \frac{2DN + (D + 1)(N^2 + N)}{(2D + 1)(N^2 + N)} = \frac{1 + D^{-1}}{2 + D^{-1}} + \frac{2D}{(2D + 1)(N + 1)} \quad (14)$$

$$S_{\text{even}} = \frac{2(D - 1)N + (D + 1)(N^2 + N)}{2D(N^2 + N)} = \frac{1 + D^{-1}}{2} + \frac{D - 1}{D(N + 1)} \quad (15)$$

It can be observed that both sparsify to 50% asymptotically as $N, D \rightarrow \infty$, thereby considerably reducing the memory footprint and computation. This is not a sparse approximation, but an analytical equivalence under this orthogonal basis transform, offering significant overhead improvements. The formulas serve as upper bounds that may be improved with JSO and/or approximation of the function.

2.3 Left-Sided Neuroadaptation

Requiring only left-sided partial diagonalisation, neuroadaptation can be described for this parameterisation. Neurogenesis involves the maintenance of ‘scaffold’ neurons, a function-invariant modification to network parameters. Neurodegeneration closely approximates function invariance, given the introduction of a new parameter: the ‘intrinsic length’, capable of absorbing residual bias.

Beginning with the addition of scaffold neurons, this neurogenesis process is achieved by embedding the existing \mathbb{R}^n activation space into \mathbb{R}^{n+1} . Considering the typical interpretation: if neurons are individuated on an arbitrary basis, this corresponds to appending additional neurons to this layer, which are connected in such a manner that the model is functionally independent of them — these could be considered ‘scaffold neurons’ in this conventional individuated picture. Alternatively, it is comparable to a further increase in the dimensionality of the generalised notion of a neuron.

Such embedding appears largely arbitrary, yet the initialisation may, in practice, involve nuances ranging from explicit to spontaneous symmetry breaking in the new neuron’s associated parameters. This raises implications for further learning related to the aforementioned optimiser-based symmetry breaking under orthogonal transforms. In any case, the new singular values should be zeroed, despite a freedom in the corresponding new row of \mathbf{W}'_3 denoted in Eqn. 13 for forward growth.

Neurodegeneration is the reverse process of producing a well-chosen subspace with appropriate reparameterisations to closely approximate function-invariance. Considering the ordered, positive singular value parameters, as one ‘neuron’ tends to zero, it becomes increasingly independent of the preceding layer — a *isotropic* normaliser, App. B, may be used to prevent magnitude-compensations in subsequent layers. Thus, pruning its corresponding entries can be achieved by removing both the outgoing connection and the neuron, given the one-to-one dependence. The thresholding of the zero-tending singular value can be selected to produce a suitably minimal degradation to model functionality. However, a singular-value-independent bias parameter persists.

A novel parameter, the scalar “intrinsic length” denoted o , is a crucial insight restoring a full neurodegeneration symmetry in the $\Lambda_{ii} \rightarrow 0$ limit. It transforms under pruning to gauge away the troublesome residual bias. The diagonalised layer, with this novel parameter, can be expressed as Eqn. 16, with Eqn. 17 displaying the restored symmetry as the limit of $\Lambda_{00} \rightarrow 0$, provided the bias in the linear term is absorbed into the next layer’s biases appropriately. Intrinsic length’s transform also preserves any existing positivity; if desired, it may be parameterised as such, e.g. $o = \exp \lambda$.

$$\mathbf{f}(\vec{x}) = \bar{\sigma} \left(\left\| \Lambda \vec{x} + \vec{b} \right\|_2^2 + o \right) \left(\Lambda \vec{x} + \vec{b} \right) \quad (16)$$

$$\left\| \mathbf{\Lambda} \vec{x} + \vec{b} \right\|_2^2 + o = \sum_{j \neq 0} (\mathbf{\Lambda}_{jj} x_j + b_j)^2 + \underbrace{(\mathbf{\Lambda}_{00} x_0 + b_0)^2}_{\rightarrow 0} + o = \left\| \mathbf{\Lambda}' \vec{x} + \vec{b}' \right\|_2^2 + \underbrace{b_0^2}_{=o} + o \quad (17)$$

This truly neurodegenerates the architecture, entering the functional class of narrower-width multi-layer perceptrons, with the reparameterisation symmetry restored in the limit, and arbitrarily well approximated by chosen thresholding. Furthermore, to counteract the persistent growth of the intrinsic length, it can be made trainable. This may offer broader benefits, such as optimising the non-linearity’s action or, if negative, allowing a non-linear sign change to representations, thereby permitting antipodal arrangements that may be desirable [23]. Numerous interpretations arise for it, such as a parameterised isotropic activation function preserving orthogonal equivariance, or a new affine translation, embedding the subspace of activations away from the origin, by a rotationally-degenerate bias-like vector in the orthogonal complement space, constrained by $\vec{\sigma}^T \vec{\sigma} = o$ and $\vec{\sigma} \perp \mathbf{\Lambda} \vec{x} + \vec{b}$.

Additionally, this forward correction for the residual bias in the linear term is similarly applicable to any remaining $\mathbf{\Lambda}_{ii} = \epsilon$ by application of a Moore-Penrose pseudo-inverse. Given diagonalised weights $\mathbf{\Lambda}$ and the subsequent pruned form $\mathbf{\Lambda}'$ alongside the next layer’s weight matrices before (\mathbf{W}) and after pruning (\mathbf{W}'), then the following map should be closely preserved: $\mathbf{W}' \mathbf{\Lambda}' \vec{x} \approx \mathbf{W} \mathbf{\Lambda} \vec{x}$. Determining \mathbf{W}' through pseudo-inverse, such as to minimise a least-squares difference in these maps. Where rank permits, one can then use Eqn. 18 — otherwise continue using classically pruned \mathbf{W}' . This also becomes problematic if the threshold is particularly small, which may lead to a poorly-conditioned inverse and necessitate careful use of this method. In the standard case of the smallest singular value deletion, this reduces to a simple corresponding column deletion of \mathbf{W}' .

$$\mathbf{W}' = \mathbf{W} \mathbf{\Lambda} \mathbf{\Lambda}'^T \left(\mathbf{\Lambda}' \mathbf{\Lambda}'^T \right)^{-1} \quad (18)$$

2.3.1 Neurogenesis and Jacobians of Isotropic Activation Functions

Any concerns regarding the trainability of new scaffold neurons are mitigated by analysing the Jacobian of the isotropic activation function, and App. A.3’s discussion. Alongside standard connectivity mixing, these non-elementwise Jacobians distribute learning gradients globally even in the case of an effective activation subspace. Hence, apparent ‘neurons’ may be trained rapidly, even when independent of the model’s function, due to zero-valued associated parameters. The ‘I term’ in the isotropic Jacobian of Eqn. 19, is generally non-zero; this last entry is zeroed in the elementwise Jacobian of Eqn. 20. Merely a coordinate singularity exists at $\vec{0}$ under a suitable choice of $\vec{\sigma}$.

$$\mathbf{f}(\vec{x}) = \vec{\sigma}(\|\vec{x}\|_2) \vec{x} \quad \Rightarrow \quad J_{\mathbf{f}} = \vec{\sigma}(\|\vec{x}\|_2) \mathbf{I} + \frac{\vec{\sigma}'(\|\vec{x}\|_2)}{\|\vec{x}\|_2} \vec{x} \vec{x}^T \quad (19)$$

$$\mathbf{f}(\vec{x}) = \sum_{i=1}^n \sigma(\vec{x} \cdot \hat{e}_i) \hat{e}_i \quad \Rightarrow \quad J_{\mathbf{f}} = \sum_{i=1}^n \sigma'(\vec{x} \cdot \hat{e}_i) \hat{e}_i \hat{e}_i^T \quad (20)$$

This increases gradient flow through scaffold neurons, hastening differentiation and operationalisation.

2.3.2 Practical Considerations of Scheduling and Thresholding

Singular value decomposition itself features a $\mathcal{O}(m^2 n)$ computational scaling dependence for $\mathbb{R}^{n \times m}$, $m < n$, matrices. Due to this cost, it is appropriate to consider only intermittent scheduling for neuroadaptation. Such scheduling aligns with existing literature [17], yet here it results from the computational cost of the SVD rather than from the dense gradient computation. For straightforward implementation, this work considers layerwise decomposition only once per epoch.

Similarly, a suitable threshold, $0 < \vartheta < 1$, should be chosen to demarcate where singular values are considered negligible or rarely contributing, and above it are significant to the model function. One could also examine whether rarely significant connections tend to produce non-robust maladaptations. A further hyperparameter is the quantity of buffered scaffold neurons in the diagonalised representation maintained, $\Xi \in \mathbb{Z}_+$, whose singular values fall below the threshold. Due to the non-elementwise nature of isotropic activation functions, various values for Ξ are inequivalent, resulting in tangible training and inference differences. A learning-induced increase in scaffold neurons in the buffer then triggers neurodegeneration, removing the smallest singular-value neuron of least impact; an insufficient number triggers neurogenesis — offering a principled, real-time network adaptability.

Alternatives to assessing (diagonalised-)neuron importance can generalise this approach; it is not considered the only possibility. The magnitude of the gradient with respect to the loss [16] may be considered, among others; however, constant, predefined growth and pruning should be avoided due to the repeated replacement of small singular values — a reactive implementation is required.

2.3.3 Algorithmic Implementation

This section lists the exact transforms required for a forward neuroadaptation for an isotropic layer map $\mathbb{R}^n \rightarrow \mathbb{R}^m \rightarrow \mathbb{R}^p$, producing a varying m . Several steps and reparameterisations can be contracted for efficiency, meaningfully altering the optimisation trajectories, discussed in *App. A*.

At a time determined by the chosen scheduler, and to be repeated per layer specified, perform the left-sided partial diagonalisation stated in *Eqn. 21* — such diagonalisation needn't be later undone. From the diagonalised singular value matrix, $\mathbf{\Lambda}$, determine the number of singular values, below the specified threshold $\mathbf{\Lambda}_{ii} < \vartheta$, which defines the number of scaffold neurons.

$$\mathbf{f}(\vec{x}) = \mathbf{W}_2 f_{\text{Iso}}(\mathbf{\Lambda} \mathbf{Q}^T \vec{x} + \vec{b}_1; o) + \vec{b}_2 \quad (21)$$

If the number of scaffold neurons falls below the desired count $\omega = |\{\mathbf{\Lambda}_{ii} | \mathbf{\Lambda}_{ii} < \vartheta\}| < \Xi$, iteratively enact neurogenesis for $(\Xi - \omega)$ neurons, described as follows:

1. Append a row of zeros to the bottom of $\mathbf{\Lambda} \in \mathbb{R}_{\geq 0}^{m \times n}$, to form a matrix $\mathbf{\Lambda}' \in \mathbb{R}_{\geq 0}^{(m+1) \times n}$.
2. For $\vec{b}_1 \in \mathbb{R}^m$ this is expanded to include a new last entry, b_* to form $\vec{b}'_1 \in \mathbb{R}^{(m+1)}$. For o -positivity, b_* must be chosen such that $b_*^2 + o' = o$, while $b_* = 0$ is needed for \vec{b}_2 step.
3. Hence, with $o \in \mathbb{R}_{\geq 0}$, an adjustment follows accordingly from the prior step: $o' = o - b_*^2$.
4. The weight matrix, $\mathbf{W}_2 \in \mathbb{R}^{p \times m}$, acquires a new column, \vec{W}_* , forming $\mathbf{W}_2 \in \mathbb{R}^{p \times (m+1)}$. The column \vec{W}_* exhibits freedom in its initialisation only during the forward pass, due to zero premultiplication; however, it does couple with the optimisation discussed below.
5. For vector, $\vec{b}_2 \in \mathbb{R}^p$, no adjustment needs to be made, if $b_* = 0$, due to identical impact.

Initialising \vec{W}_* as the (near-)zero vector will result in spontaneous symmetry breaking in the next optimisation step, whilst a non-zero vector acts as an explicit symmetry breaking, biasing learning accordingly, discussed in *App. A.3*. Hence, a range of options is available for empirical exploration: a linear combination of existing columns to achieve greater fidelity around the existing span, or various choices for semi-orthogonality, etc. Choices about symmetry-breaking initialisations may result in scaffold neurons diverging in specialisation, with their number having significant consequences.

Iterative pruning occurs when the number of scaffold neurons exceeds the desired count, $\omega > \Xi$.

1. The row of $\mathbf{\Lambda} \in \mathbb{R}_{\geq 0}^{m \times n}$ with smallest norm is deleted, forming $\mathbf{\Lambda}' \in \mathbb{R}_{\geq 0}^{(m-1) \times n}$.
2. Similarly, delete the corresponding entry, b_* , of $\vec{b}_1 \in \mathbb{R}^m$ to form $\vec{b}'_1 \in \mathbb{R}^{(m-1)}$.
3. Adjust $o \in \mathbb{R}_{\geq 0}$ accordingly by $o' = o + b_*^2$.
4. Deletion of $\mathbf{W}_2 \in \mathbb{R}^{p \times m}$ corresponding column, \vec{W}_* , then yields $\mathbf{W}_2 \in \mathbb{R}^{p \times (m-1)}$.
5. For vector, $\vec{b}_2 \in \mathbb{R}^p$, an adjustment arising from the prior bias term can be considered: $\vec{b}'_2 = \vec{b}_2 + \mathbb{E}[\bar{\sigma}(\cdot)] \vec{W}_* b_*$. This better approximates the functionality, where the expectation may be computed batch-wise or test-set-wise, or if isotropic normalisation ensures it is one.

Better still, a further non-linear additive term and learnable parameter, $+\sigma(\cdot) \vec{\psi}$, can be used to absorb such terms identically, $\vec{\psi}' = \vec{\psi} + \vec{W}_* b_*$ — essential is its regularised decay $\vec{\psi} \rightarrow \vec{0}$. This is for two reasons: it must be negligible before next-layer pruning, so it doesn't require further correction, and this also suggests an output-to-input ordering for neuroadaptation. Secondly, translation inconsistency due to the non-linear behaviour of ψ may be troublesome, so it should decay over a short yet sufficient time for the network to compensate appropriately. Across both procedures, $\mathbf{Q}^T \in \mathbb{R}^{n \times n}$, needn't be changed and can then be contracted with $\mathbf{\Lambda}'$ once concluded. Repeating this procedure over all specified layers then produces the automatic adaptive architecture. One can choose the final layer representations, but alternating diagonalisation may be beneficial for the aforementioned sparsity.

3 Empirical Verifications of Theory and Mechanisms

Naturally, the present derivations apply to multilayer perceptrons; hence, the claims must be assessed in reference to this architecture only — despite the precedence of transformer [34] and convolution SOTA. Similarly, the objective is to empirically verify the theoretical claims regarding function invariance and neuroadaptation, rather than overall competitiveness. Thus, $\sigma(a) = \tanh a$ is used as a working placeholder, in analogy to standard-tanh, but is not assumed to be implicitly optimal¹.

Table 1: Experiment One (*App. I.1*): demonstrates the effect of neuroadaptation on a network, by appending or removing diagonalised neurons from the initial $\mathbb{R}^{100} \rightarrow \mathbb{R}^{100}$ affine layer in a [3072, 100, 100, 10] CIFAR-10 trained classifier over 20 independent repeats. Each column specifies an approach for the intrinsic length o and the ψ -vector, yielding 7×20 unique networks. Notated Σ_0 for the mean initial sum of the layer’s singular values, and Σ_1 for the sum after neuroadaptation, and ϵ for the mean per-example L_2 -distance between the classifier logits before and after neuroadaptation.

Neuroadaptation	Omniscient, $\vec{v}_{\text{Omniscient}}$		Omniscient, $\vec{v}_{\text{Omniscient}}$		Omniscient, $\vec{v}_{\text{Omniscient}}$		Omniscient, $\vec{v}_{\text{Omniscient}}$		Omniscient, $\vec{v}_{\text{Omniscient}}$		Omniscient, $\vec{v}_{\text{Omniscient}}$		Omniscient, $\vec{v}_{\text{Omniscient}}$	
	$\Sigma_0 = (0.174 \pm 0.001) \times 10^3$	$\Sigma_0 = (0.174 \pm 0.001) \times 10^3$	$\Sigma_0 = (0.174 \pm 0.001) \times 10^3$	$\Sigma_0 = (0.174 \pm 0.001) \times 10^3$	$\Sigma_0 = (0.174 \pm 0.001) \times 10^3$	$\Sigma_0 = (0.174 \pm 0.001) \times 10^3$	$\Sigma_0 = (0.164 \pm 0.001) \times 10^3$	$\Sigma_0 = (0.164 \pm 0.001) \times 10^3$	$\Sigma_0 = (0.164 \pm 0.001) \times 10^3$	$\Sigma_0 = (0.164 \pm 0.001) \times 10^3$	$\Sigma_0 = (0.174 \pm 0.001) \times 10^3$	$\Sigma_0 = (0.174 \pm 0.001) \times 10^3$	$\Sigma_0 = (0.174 \pm 0.001) \times 10^3$	$\Sigma_0 = (0.174 \pm 0.001) \times 10^3$
	$\epsilon (10^{-4})$	$\Sigma_1 (10^3)$	$\epsilon (10^{-4})$	$\Sigma_1 (10^3)$	$\epsilon (10^{-4})$	$\Sigma_1 (10^3)$	$\epsilon (10^{-4})$	$\Sigma_1 (10^3)$	$\epsilon (10^{-4})$	$\Sigma_1 (10^3)$	$\epsilon (10^{-4})$	$\Sigma_1 (10^3)$	$\epsilon (10^{-4})$	$\Sigma_1 (10^3)$
75	2 ± 0	0.174 ± 0.001	2 ± 1	0.174 ± 0.001	2 ± 0	0.174 ± 0.001	2 ± 0	0.174 ± 0.001	1 ± 0	0.164 ± 0.001	1 ± 0	0.164 ± 0.001	1 ± 0	0.174 ± 0.001
50	2 ± 0	0.174 ± 0.001	2 ± 1	0.174 ± 0.001	2 ± 0	0.174 ± 0.001	2 ± 0	0.174 ± 0.001	1 ± 0	0.164 ± 0.001	1 ± 0	0.164 ± 0.001	1 ± 0	0.174 ± 0.001
25	2 ± 0	0.174 ± 0.001	2 ± 1	0.174 ± 0.001	2 ± 0	0.174 ± 0.001	2 ± 0	0.174 ± 0.001	1 ± 0	0.164 ± 0.001	1 ± 0	0.164 ± 0.001	1 ± 0	0.174 ± 0.001
5	2 ± 0	0.174 ± 0.001	2 ± 1	0.174 ± 0.001	2 ± 0	0.174 ± 0.001	2 ± 0	0.174 ± 0.001	1 ± 0	0.164 ± 0.001	1 ± 0	0.164 ± 0.001	1 ± 0	0.174 ± 0.001
1	2 ± 0	0.174 ± 0.001	2 ± 1	0.174 ± 0.001	2 ± 0	0.174 ± 0.001	2 ± 0	0.174 ± 0.001	1 ± 0	0.164 ± 0.001	1 ± 0	0.164 ± 0.001	1 ± 0	0.174 ± 0.001
0	2 ± 0	0.174 ± 0.001	2 ± 1	0.174 ± 0.001	2 ± 0	0.174 ± 0.001	2 ± 0	0.174 ± 0.001	1 ± 0	0.164 ± 0.001	1 ± 0	0.164 ± 0.001	1 ± 0	0.174 ± 0.001
-1	2 ± 2	0.174 ± 0.001	2 ± 1	0.174 ± 0.001	2 ± 0	0.174 ± 0.001	22 ± 22	0.174 ± 0.001	2 ± 1	0.164 ± 0.001	2 ± 1	0.164 ± 0.001	5 ± 5	0.174 ± 0.001
-5	52 ± 22	0.174 ± 0.001	33 ± 13	0.174 ± 0.001	33 ± 15	0.174 ± 0.001	310 ± 173	0.174 ± 0.001	25 ± 10	0.164 ± 0.001	27 ± 9	0.164 ± 0.001	86 ± 44	0.174 ± 0.001
-25	772 ± 74	0.162 ± 0.001	621 ± 66	0.162 ± 0.001	627 ± 59	0.162 ± 0.001	2656 ± 554	0.162 ± 0.001	715 ± 56	0.152 ± 0.001	706 ± 71	0.152 ± 0.001	890 ± 78	0.162 ± 0.001
-50	890 ± 80	0.139 ± 0.001	695 ± 62	0.139 ± 0.001	699 ± 53	0.139 ± 0.001	3015 ± 552	0.139 ± 0.001	794 ± 59	0.130 ± 0.001	793 ± 76	0.130 ± 0.001	1007 ± 87	0.139 ± 0.001
-75	1028 ± 94	0.115 ± 0.001	801 ± 64	0.114 ± 0.001	809 ± 57	0.115 ± 0.001	3471 ± 642	0.115 ± 0.001	907 ± 62	0.105 ± 0.001	902 ± 82	0.105 ± 0.001	1168 ± 99	0.115 ± 0.001

One can observe that constant or trainable intrinsic length ‘ o ’ and, especially, $\vec{\psi}$ produced the best invariances throughout the experiment, with $\epsilon \approx 10^{-4}$ indicating negligible alteration of the function. Considering that *no retraining* occurred subsequent to the neuroadaptation explains the consistency between constant and trainable o and $\vec{\psi}$ results. Even for relatively large neurodegeneration, e.g., -75 for width $100 \rightarrow 25$ with trainable compensatory parameters, it still resulted in very small error in logit output, $\epsilon = 0.09$. Thus, these networks, up to propagation of machine precision, may be considered to remain identically invariant under neurogenesis and diagonalisation (0 row), whilst being very well approximated for neurodegeneration, all predicted by the symmetry-led construction.

Training-set optimisation, at 19.0 ± 0.2 s, and test-set evaluation, at 2.04 ± 0.01 s, made the epoch-wise diagonalisation and neurogenesis, 29 ± 1 ms, or neurodegeneration, 39 ± 2 ms, negligible compared to the computation of the training and evaluation passes.

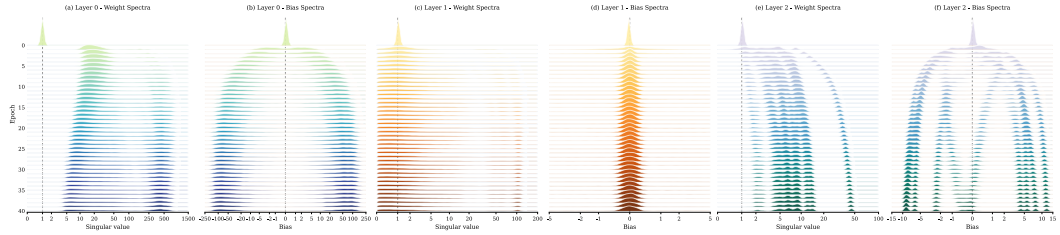


Figure 2: Experiment Two (*App. I.2*) displays the evolving layerwise singular value and bias spectra for a [3072, 100, 100, 10] fixed isotropic MLP trained on CIFAR10 [35] classification. The spectra are obtained from 40 independent repeats, showing strong consistency. Singular values begin at one, indicated by the dashed line, due to orthogonal initialisation, and biases at zero due to initialisation.

Fig. 2 shows that the isotropic networks evolve in a very comparable manner despite random (orthogonal) initialisation. This may be due to the inherent symmetry producing a flat-loss curve about the continuous group orbits. Strong specialisation is observed in layers 0 and 2, with subsequent decay in parts of the spectra — encouraging, when adaptive, neurodegeneration of unused parameters. *Fig. 3* demonstrates that, on average, neurogenesis proceeds, and frequently stabilises, with each

¹‘Isotropic-tanh’ also saturates, $\lim_{\alpha \rightarrow \infty} \sigma(\alpha) = 1$, which alleviates concerns regarding magnitude growth in activations compensating for small singular values. Thus, zero-tending singular values do suggest a negligible contribution to the function.

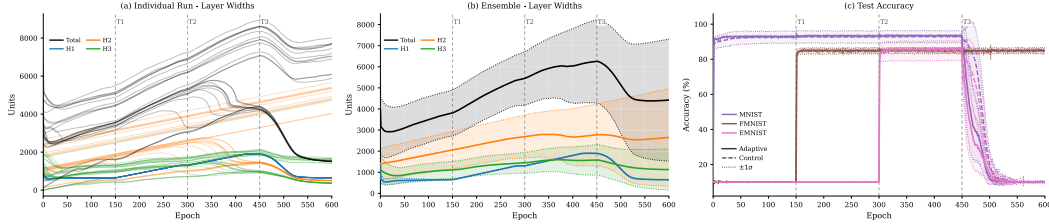


Figure 3: Experiment Three (*App. I.3*) demonstrates thresholded neural adaptation when an architecture of $[2352, H1, H2, H3, 30]$ adapts to a changing task schedule, across 25 independent repeats for random hidden widths $H1, H2, H3 \sim U(500, 2500)$. From epoch 0 through 150, only MNIST [36] cross-entropy terms contribute to the loss; at T1, the total loss is equally averaged between both MNIST and FMNIST [37]. At T2, the total loss is equally averaged between both MNIST, FMNIST, and A-J letters from EMNIST [38] contribute, and finally T3, *only* FMNIST’s loss contributes.

appended task, followed by a neurodegeneration trend to a stable value after tasks are removed. Degradation of FMNIST and MNIST test accuracies was intended due to parameter decay, but singular values may be frozen to prevent function loss. Thresholded scaffold neurons operate as desired, exiting the buffer when required for new tasks, triggering neurogenesis, and otherwise decaying and neurodegenerating excess when unneeded. Such decay is evident in *Fig. 2*, particularly subplots ‘a’ and ‘f’. Adaptive networks have improved accuracy compared to static baselines².

Curiously, a bifurcation appears for H2 and H3 beginning during the T2 schedule: either continued neurogenesis proceeds, or rapid convergence to a stable value is observed. Speculated to be a function consolidation, in which inter-task learning transfer merges separately acquired task-specific behaviours into a shared approach supporting the multiple tasks — reducing redundancy in both function and neurons. The lower, stable merged value relative to many T2 and T3 widths is suggestive of this phenomenon, alongside the convergence prior to the T3 boundary, where the addition of EMNIST may have provided a bridging intermediate. Similarly, its occurrence in the H2 and H3 layers, rather than in H1, may indicate that redundancy is exploited in deeper, more generalised representations that are shareable across the varying tasks. Analysing individual runs also indicates that the bifurcation may involve layer couplings, typically dividing between the standard contracting $H1 \geq H2 \geq H3$ width structure, which stabilises, and $H2 \geq H3 \geq H1$, which continues to grow.

Table 2: Experiment Four (*App. I.4*) shows test accuracy for neuroadaptation between two set widths.

Start width \ End width	7	10	25	50	75	100
7	39.88±0.36	41.65±0.12	43.83±0.02	44.37±0.15	43.95±0.42	43.91±0.36
10	39.64±0.25	41.88±0.36	43.59±0.44	43.96±0.19	44.18±0.26	43.90±0.47
25	38.94±0.30	41.30±0.50	43.41±0.51	43.50±0.34	43.57±0.07	43.74±0.53
50	38.84±0.44	41.14±0.41	43.05±0.32	43.43±0.29	43.74±0.25	43.59±0.34
75	38.48±0.53	41.32±0.59	43.19±0.43	43.70±0.23	43.12±0.46	43.95±0.17
100	39.27±0.09	41.19±0.62	43.33±0.13	43.75±0.37	43.68±0.25	43.24±0.54

4 Conclusion

A symmetry-led approach to adaptive topologies was developed, using activation functions with prescribed orthogonal equivariance which permit a function-invariant diagonalising basis change. Adaptive-width isotropic multi-layer perceptrons were verified across datasets, confirming negligible functional degradation under substantial architectural adaptation. Appendices cover optimisers and normaliser considerations under orthogonal reformulation, sparsification verification, nested functional classes, ICA-representations, a sketch of convolution neuroadaptation and the *parallelised precomputation of all matrix-vector products* for isotropic networks. Scope, limitations, and related work are also discussed. Together, these results suggest that the taxonomy and reversed ontology underlying the method have practical utility, demonstrated for adaptive networks, whilst expanding the functional class of neural systems through new primitive forms and permitting new behaviours.

²At T3, epoch 450, the (control)/(adaptive) mean and standard error test accuracy, was recorded at $(92.9 \pm 0.7)\% / (93.3 \pm 0.1)\%$ for MNIST, $(84.7 \pm 0.3)\% / (85.1 \pm 0.1)\%$ for FMNIST and $(85.0 \pm 1.1)\% / (86.1 \pm 0.2)\%$ for A-J EMNIST

References

- [1] Caleb J. Axelrod, Swanne P. Gordon, and Bruce A. Carlson. Integrating neuroplasticity and evolution. *Current Biology*, 33(8):R288–R293, Apr 2023. ISSN 0960-9822. doi: 10.1016/j.cub.2023.03.002. URL <https://doi.org/10.1016/j.cub.2023.03.002>.
- [2] Wei Wen and Gina G Turrigiano. Keeping your brain in balance: homeostatic regulation of network function. *Annual review of neuroscience*, 47, 2024.
- [3] Pico Caroni, Flavio Donato, and Dominique Muller. Structural plasticity upon learning: regulation and functions. *Nature Reviews Neuroscience*, 13(7):478–490, 2012.
- [4] Jyoti Mishra and Adam Gazzaley. Cross-species approaches to cognitive neuroplasticity research. *NeuroImage*, 131:4–12, 2016. doi: 10.1016/j.neuroimage.2015.10.013. URL <https://doi.org/10.1016/j.neuroimage.2015.10.013>.
- [5] Chiara La Rosa and Luca Bonfanti. Brain plasticity in mammals: An example for the role of comparative medicine in the neurosciences. *Frontiers in Veterinary Science*, 5:274, 2018. doi: 10.3389/fvets.2018.00274. URL <https://doi.org/10.3389/fvets.2018.00274>.
- [6] Ioanna Dori, Chrysanthi Bekiari, Ioannis Grivas, Anastasia Tsingotjidou, and Georgios C Papadopoulos. Birth and death of neurons in the developing and mature mammalian brain. *The International Journal of Developmental Biology*, 66(1-2-3):9–22, 2021.
- [7] Anthony Holtmaat and Karel Svoboda. Experience-dependent structural synaptic plasticity in the mammalian brain. *Nature Reviews Neuroscience*, 10(9):647–658, 2009.
- [8] Martin M Riccomagno and Alex L Kolodkin. Sculpting neural circuits by axon and dendrite pruning. *Annual review of cell and developmental biology*, 31(1):779–805, 2015.
- [9] Carolin Scholl, Michael E Rule, and Matthias H Hennig. The information theory of developmental pruning: Optimizing global network architectures using local synaptic rules. *PLoS computational biology*, 17(10):e1009458, 2021.
- [10] Gina G Turrigiano and Sacha B Nelson. Hebb and homeostasis in neuronal plasticity. *Current opinion in neurobiology*, 10(3):358–364, 2000.
- [11] Dmitri B Chklovskii, BW Mel, and K Svoboda. Cortical rewiring and information storage. *Nature*, 431(7010):782–788, 2004.
- [12] Liyuan Wang, Xingxing Zhang, Hang Su, and Jun Zhu. A comprehensive survey of continual learning: Theory, method and application, 2024. URL <https://arxiv.org/abs/2302.00487>.
- [13] Warren S McCulloch and Walter Pitts. A logical calculus of the ideas immanent in nervous activity. *The bulletin of mathematical biophysics*, 5(4):115–133, 1943.
- [14] Song Han, Jeff Pool, John Tran, and William J. Dally. Learning both weights and connections for efficient neural networks, 2015. URL <https://arxiv.org/abs/1506.02626>.
- [15] Yiwen Guo, Anbang Yao, and Yurong Chen. Dynamic network surgery for efficient dnns, 2016. URL <https://arxiv.org/abs/1608.04493>.
- [16] Namhoon Lee, Thalaisyasingam Ajanthan, and Philip H. S. Torr. Snip: Single-shot network pruning based on connection sensitivity, 2019. URL <https://arxiv.org/abs/1810.02340>.
- [17] Utku Evci, Trevor Gale, Jacob Menick, Pablo Samuel Castro, and Erich Elsen. Rigging the lottery: Making all tickets winners, 2021. URL <https://arxiv.org/abs/1911.11134>.
- [18] Michael C Mozer and Paul Smolensky. Skeletonization: A technique for trimming the fat from a network via relevance assessment. *Advances in neural information processing systems*, 1, 1988.
- [19] Woojeong Kim, Suhyun Kim, Mincheol Park, and Geunseok Jeon. Neuron merging: Compensating for pruned neurons. *Advances in Neural Information Processing Systems*, 33:585–595, 2020.

- [20] Héctor J. Sussmann. Uniqueness of the weights for minimal feedforward nets with a given input-output map. *Neural Networks*, 5(4):589–593, 1992. ISSN 0893-6080. doi: [https://doi.org/10.1016/S0893-6080\(05\)80037-1](https://doi.org/10.1016/S0893-6080(05)80037-1). URL <https://www.sciencedirect.com/science/article/pii/S0893608005800371>.
- [21] Vijay Badrinarayanan, Bamdev Mishra, and Roberto Cipolla. Understanding symmetries in deep networks, 2015. URL <https://arxiv.org/abs/1511.01029>.
- [22] Charles Godfrey, Davis Brown, Tegan Emerson, and Henry Kvinge. On the symmetries of deep learning models and their internal representations, 2023. URL <https://arxiv.org/abs/2205.14258>.
- [23] Nelson Elhage, Tristan Hume, Catherine Olsson, Nicholas Schiefer, Tom Henighan, Shauna Kravec, Zac Hatfield-Dodds, Robert Lasenby, Dawn Drain, Carol Chen, et al. Toy models of superposition. *arXiv preprint arXiv:2209.10652*, 2022.
- [24] George Bird. The spotlight resonance method: Resolving the alignment of embedded activations. In *Second Workshop on Representational Alignment at ICLR 2025*, 2025. URL <https://openreview.net/forum?id=alxPpqVRzX>.
- [25] George Bird. Emergence of quantised representations isolated to anisotropic functions, 2025. URL <https://arxiv.org/abs/2507.12070>.
- [26] J. Héroult and B. Ans. Réseau de neurones à synapses modifiables: Décodage de messages sensoriels composites par apprentissage non supervisé et permanent. *Comptes Rendus de l'Académie des Sciences, Série III*, 299:525–528, 1984.
- [27] Bernard Ans, Jeanny Héroult, Christian Jutten, et al. Architectures neuromimétiques adaptatives: Détection de primitives. *Proceedings of Cognitiva*, 85(2):593–597, 1985.
- [28] Pierre Comon. Independent component analysis, a new concept? *Signal processing*, 36(3): 287–314, 1994.
- [29] Kunihiko Fukushima. Neocognitron: A self-organizing neural network model for a mechanism of pattern recognition unaffected by shift in position. *Biological cybernetics*, 36(4):193–202, 1980.
- [30] Yann LeCun, Bernhard Boser, John S Denker, Donnie Henderson, Richard E Howard, Wayne Hubbard, and Lawrence D Jackel. Backpropagation applied to handwritten zip code recognition. *Neural computation*, 1(4):541–551, 1989.
- [31] George Bird. Isotropic deep learning: You should consider your (foundational) biases, May 2025. URL <https://doi.org/10.5281/zenodo.15476947>.
- [32] David Bau, Bolei Zhou, Aditya Khosla, Aude Oliva, and Antonio Torralba. Network dissection: Quantifying interpretability of deep visual representations, 2017. URL <https://arxiv.org/abs/1704.05796>.
- [33] Chris Olah, Alexander Mordvintsev, and Ludwig Schubert. Feature visualization. *Distill*, 2017. doi: 10.23915/distill.00007. <https://distill.pub/2017/feature-visualization>.
- [34] Ashish Vaswani, Noam Shazeer, Niki Parmar, Jakob Uszkoreit, Llion Jones, Aidan N. Gomez, Lukasz Kaiser, and Illia Polosukhin. Attention is all you need, 2023. URL <https://arxiv.org/abs/1706.03762>.
- [35] Alex Krizhevsky, Geoffrey Hinton, et al. Learning multiple layers of features from tiny images. 2009.
- [36] Yann LeCun, Léon Bottou, Yoshua Bengio, and Patrick Haffner. Gradient-based learning applied to document recognition. *Proceedings of the IEEE*, 86(11):2278–2324, 2002.
- [37] Han Xiao, Kashif Rasul, and Roland Vollgraf. Fashion-mnist: a novel image dataset for benchmarking machine learning algorithms. *arXiv preprint arXiv:1708.07747*, 2017.

- [38] Gregory Cohen, Saeed Afshar, Jonathan Tapson, and Andre Van Schaik. Emnist: Extending mnist to handwritten letters. In *2017 international joint conference on neural networks (IJCNN)*, pages 2921–2926. IEEE, 2017.
- [39] Ilya Sutskever, James Martens, George Dahl, and Geoffrey Hinton. On the importance of initialization and momentum in deep learning. In *International conference on machine learning*, pages 1139–1147. pmlr, 2013.
- [40] Diederik P. Kingma and Jimmy Ba. Adam: A method for stochastic optimization, 2017. URL <https://arxiv.org/abs/1412.6980>.
- [41] Ilya Loshchilov and Frank Hutter. Decoupled weight decay regularization, 2019. URL <https://arxiv.org/abs/1711.05101>.
- [42] Sergey Ioffe and Christian Szegedy. Batch normalization: Accelerating deep network training by reducing internal covariate shift. In *International conference on machine learning*, pages 448–456. pmlr, 2015.
- [43] Jimmy Lei Ba, Jamie Ryan Kiros, and Geoffrey E Hinton. Layer normalization. *arXiv preprint arXiv:1607.06450*, 2016.
- [44] Biao Zhang and Rico Sennrich. Root mean square layer normalization. *Advances in neural information processing systems*, 32, 2019.
- [45] Kaiming He, Xiangyu Zhang, Shaoqing Ren, and Jian Sun. Deep residual learning for image recognition. In *Proceedings of the IEEE conference on computer vision and pattern recognition*, pages 770–778, 2016.
- [46] Frank Rosenblatt. The perceptron: a probabilistic model for information storage and organization in the brain. *Psychological review*, 65(6):386, 1958.
- [47] George Cybenko. Approximation by superpositions of a sigmoidal function. *Mathematics of control, signals and systems*, 2(4):303–314, 1989.
- [48] Sara Sabour, Nicholas Frosst, and Geoffrey E Hinton. Dynamic routing between capsules, 2017. URL <https://arxiv.org/abs/1710.09829>.
- [49] David S Broomhead and David Lowe. Radial basis functions, multi-variable functional interpolation and adaptive networks. Technical report, 1988.
- [50] Derek Lim, Theo Moe Putterman, Robin Walters, Haggai Maron, and Stefanie Jegelka. The empirical impact of neural parameter symmetries, or lack thereof, 2024. URL <https://arxiv.org/abs/2405.20231>.
- [51] Tianqi Chen, Ian Goodfellow, and Jonathon Shlens. Net2net: Accelerating learning via knowledge transfer, 2016. URL <https://arxiv.org/abs/1511.05641>.
- [52] Tao Wei, Changhu Wang, Yong Rui, and Chang Wen Chen. Network morphism. In *International conference on machine learning*, pages 564–572. PMLR, 2016.
- [53] Jonathan Frankle and Michael Carbin. The lottery ticket hypothesis: Finding sparse, trainable neural networks, 2019. URL <https://arxiv.org/abs/1803.03635>.
- [54] Ilya Loshchilov and Frank Hutter. Decoupled weight decay regularization. *arXiv preprint arXiv:1711.05101*, 2017.
- [55] Adam Paszke, Sam Gross, Francisco Massa, Adam Lerer, James Bradbury, Gregory Chanan, Trevor Killeen, Zeming Lin, Natalia Gimelshein, Luca Antiga, Alban Desmaison, Andreas Köpf, Edward Yang, Zach DeVito, Martin Raison, Alykhan Tejani, Sasank Chilamkurthy, Benoit Steiner, Lu Fang, Junjie Bai, and Soumith Chintala. Pytorch: An imperative style, high-performance deep learning library, 2019. URL <https://arxiv.org/abs/1912.01703>.
- [56] Gregory Griffin, Alex Holub, and Pietro Perona. Caltech-256 object category dataset. 2007.

A Considering Gradient Non-Invariance

Despite the forward-pass invariance of various reparameterisation approaches, some reparameterisations diverge in their optimisation trajectories under these transforms. This section will overview these considerations.

A.1 Transforming Optimiser States

Practically, the core consideration is of the various optimiser states. These include the momentum of momentum gradient descent [39], the first- and second-order moment moving-average estimates of the ADAM [40] and ADAM-W [41] optimisers, among many others. Several can be exactly transformed under a basis change to ensure invariance; however, some must be approximated. This requires consideration of each mathematical formulation and its motivation to determine which tensor rank the state should transform under. This section will consider derivations of the momentum and ADAM state transforms.

For simplicity, consider a vector parameter, \vec{a} , being updated by an optimiser of form $\vec{a}_{n+1} = \vec{a}_n - \eta \vec{U}(\vec{a}_n)$. Assume the network of interest has a construction such that it exhibits the forward pass invariance to orthogonal transforms on the parameter \vec{a} , $\vec{a}' = \mathbf{R}\vec{a}$. For the isotropic example, this transform is compensated for, elsewhere, as described in *Sec. 2.2*. Due to such function invariance, the loss is similarly invariant $\mathcal{L}'(\vec{a}') = \mathcal{L}(\vec{a})$ if any additional terms are assumed also invariant, such as regularisers, e.g. $\mathcal{L}_2 \propto \vec{a}^T \vec{a}$.

Therefore, to ensure continued invariance under this reparameterisation, $\mathcal{L}'(\vec{a}') = \mathcal{L}(\vec{a}_n)$, for all n , requires the trajectories to be equivariant to the reparameterisation transform. This is described in *Eqn. 22*, and effectively derives *Eqn. 1* applied to a general optimiser.

$$\vec{a}'_{n+1} = \left(\vec{a}'_n - \eta \vec{U}'(\vec{a}'_n) \right) = \left(\mathbf{R}\vec{a}_n - \eta \mathbf{R}\vec{U}(\mathbf{R}^T \vec{a}'_n) \right) = \mathbf{R}\vec{a}_{n+1} \quad \Rightarrow \quad \vec{U}'(\vec{a}') = \mathbf{R}\vec{U}(\mathbf{R}^T \vec{a}') = \mathbf{R}\vec{U}(\vec{a}) \quad (22)$$

Hence, network and loss invariance under an orthogonal transform induces an optimiser algebraic-equivariance condition, $\vec{U}'(\vec{a}') = \mathbf{R}\vec{U}(\vec{a})$. This is trivially satisfied by standard gradient descent, due to the chain rule.

$$\vec{U}'(\vec{a}') \equiv \nabla_{\vec{a}'} \mathcal{L}'(\vec{a}') = \left(\frac{\partial \vec{a}'}{\partial \vec{a}} \right)^{-T} \nabla_{\vec{a}} \mathcal{L}(\vec{a}) = \mathbf{R} \nabla_{\vec{a}} \mathcal{L}(\vec{a}) = \mathbf{R}\vec{U}(\vec{a}) \quad (23)$$

Overall, this can be understood intuitively: if $\nabla_{\varrho} \mathcal{L}$ is locally the direction of steepest descent in parameter space, for parameter ϱ , then transforming to a new orthonormal basis in parameter-space, $\varrho' = \mathbf{R}\varrho$, does not change the vector of steepest descent, only its representation in the chosen basis — the underlying loss-surface is invariant due to function invariance.

However, this must be reevaluated for momentum, $\vec{U}_{\text{mome.}}$, and ADAM optimisers, \vec{U}_{ADAM} . For momentum, with factor $\alpha \in [0, 1]$, this requires a transform to the update vector as $\vec{M}'_n = \mathbf{R}\vec{M}_n$. Hence, this transforms the same as the underlying parameter, \vec{a} , as may be expected.

$$\vec{U}_{\text{mome.}} = \vec{M}_n \quad , \quad \vec{M}_{n+1} = \alpha \vec{M}_n + (1 - \alpha) \nabla_{\vec{a}} \mathcal{L}(\vec{a}) \quad (24)$$

$$\text{requiring: } \vec{M}'_{n+1} = \mathbf{R}\vec{M}_{n+1} = \alpha \mathbf{R}\vec{M}_n + (1 - \alpha) \underbrace{\mathbf{R} \nabla_{\vec{a}} \mathcal{L}(\vec{a})}_{\nabla_{\vec{a}'} \mathcal{L}'(\vec{a}')} \quad (25)$$

For ADAM, the first moment transforms, \vec{M} identically, $\vec{M}'_n = \mathbf{R}\vec{M}_n$; however, the second moment itself is a diagonal approximation of a true second moment due to elementwise approximations. *Eqn. 26* displays ADAM in elementwise form, with the ε -positivity term neglected for simplicity.

$$\vec{U}_{\text{ADAM}} = \sum_i \frac{\vec{M}_n \cdot \hat{e}_i}{\sqrt{\vec{V}_n \cdot \hat{e}_i}} \hat{e}_i \quad \left\{ \begin{array}{l} \vec{M}_{n+1} = \beta_1 \vec{M}_n + (1 - \beta_1) \nabla_{\vec{a}} \mathcal{L}(\vec{a}) \\ \vec{V}_{n+1} = \beta_2 \vec{V}_n + (1 - \beta_2) (\nabla_{\vec{a}} \mathcal{L}(\vec{a}) \odot \nabla_{\vec{a}} \mathcal{L}(\vec{a})) \end{array} \right. \quad (26)$$

This product of gradients term in \vec{V}_n behaves as the diagonal of a rank-2 tensor quantity in terms of transform: $\tilde{V} = (\nabla_{\vec{a}}\mathcal{L}(\vec{a}) \odot \nabla_{\vec{a}}\mathcal{L}(\vec{a})) = \text{diag}\left(\nabla_{\vec{a}}\mathcal{L}(\vec{a}) (\nabla_{\vec{a}}\mathcal{L}(\vec{a}))^T\right)$, considering that it is a projection of the outer product of two rank-1 tensors. This elementwise squaring induces basis dependence by removing off-diagonal information, which is irrecoverable. Hence it is proposed to transform it as a rank-2 matrix but preserve the off-diagonal zero projection, as shown in Eqn. 27, where $\mathbf{R}^{\odot 2} = \mathbf{R} \odot \mathbf{R}$ is the an elementwise squaring of the matrix, $\text{diag} : \mathbb{R}^{n \times n} \rightarrow \mathbb{R}^n$ is the canonical diagonal function which extracts the matrix diagonal into a vector, and the reverse process $\text{diag}^\dagger : \mathbb{R}^n \rightarrow \mathbb{R}^{n \times n}$ which embeds a vector along a matrix diagonal.

$$\tilde{V}' = \text{diag}\left(\mathbf{R}\left(\text{diag}^\dagger \tilde{V}\right)\mathbf{R}^T\right) = \mathbf{R}^{\odot 2}\tilde{V} = (\mathbf{R} \odot \mathbf{R})\tilde{V} \quad (27)$$

For hyperoctahedral-prescribed networks, including the more typical permutation-prescribed networks, all these optimiser transforms are exact and consistent with a (signed) relabelling. This includes ADAM's second moment. Hence, typically, networks do not exhibit a distinction between the forward pass reparameterisation symmetry contrasted with a backward pass broken reparameterisation symmetry; their optimisation trajectories remain equivariant and exhibit a training-time function invariance, $\vec{a}'_n = \mathbf{P}\vec{a}_n$, for all n and constant permutation matrix \mathbf{P} . Yet this is not the case for orthogonal transforms; the second-moment transform is only approximate. The network is symmetric under orthogonal reparameterisations during the forward pass, but it couples with certain optimisers in a non-invariant manner, such that reparameterisations yield different optimisation trajectories.

Nevertheless, one should still apply the approximate transform to ADAM's second moment to avoid inappropriate scaling of the effective loss surface, and it is proposed that this approximated rank-2 transform is more consistent with the quadratic gradient term than treating it as a rank-1 quantity $\vec{V}' = \mathbf{R}\vec{V}$. Hence, an inference-time reparameterisation orthogonal symmetry exists, but concurrently, a training-time equivalent symmetry does not generally exist.

Overall, the practical takeaway is that, provided an optimiser is equivariant under the symmetry and the function and loss are invariant under it, an appropriate reparameterisation of the model and optimiser yields an equivariant trajectory.

A.2 Tensor Contraction Inequivilance

A separate, classical, route in which reparameterisation can result in a function-invariance but optimiser non-invariance is considering the presence and absence of various tensor contractions, such as whether the SVD decomposition preserves $\mathbf{A}\mathbf{Q}^T$ as separate or contracted $\mathbf{W}' = \mathbf{A}\mathbf{Q}^T$. This consideration is more broadly pertinent, including implications for the normaliser's constrained-affine parameterised maps. Generally, this arises when optimisation is performed on the parameter space, with these non-contracted maps increasing dimensionality, thereby altering the loss surface and steepest descent, resulting in different optimiser trajectories.

Considering the map $\vec{y}_m = \mathbf{W}_{mn}\vec{x}_n$ with decomposition $\mathbf{A}\mathbf{B} = \mathbf{W}$, one can see two different functions after a gradient step when assuming standard gradient descent and notation $\vec{g} = \nabla_{\varrho}\mathcal{L}$ for appropriate parameter ϱ .

$$\vec{y}'_m = (\mathbf{W}_{mn} - \eta\vec{g}_m\vec{x}_n)\vec{x}_n \quad \Rightarrow \quad \Delta\vec{y} = \vec{y}' - \vec{y} = -\eta\|\vec{x}\|_2^2\vec{g} \quad (28)$$

$$\vec{y}'_m = (\mathbf{A}_{mk} - \eta\vec{g}_m\mathbf{B}_{ki}\vec{x}_i)(\mathbf{B}_{kn} - \eta\vec{g}_j\mathbf{A}_{jk}\vec{x}_n)\vec{x}_n \quad (29)$$

$$\Rightarrow \quad \Delta\vec{y} = \vec{y}' - \vec{y} = -\eta\left(\vec{g}\|\mathbf{B}\vec{x}\|_2^2 + \|\vec{x}\|_2^2\mathbf{A}\mathbf{A}^T\vec{g}\right) + \eta^2\|\vec{x}\|_2^2(\vec{x}^T\mathbf{B}^T\mathbf{A}^T\vec{g})\vec{g} \quad (30)$$

This result shows that leaving a layer in a *decomposed* diagonalised parameterisation leads to differences in optimisation.

A.3 Null-Like Reparameterisations

Of greater significance for this paper are the null-like reparameterisations that arise when the singular values of a partially or fully diagonalised layer tend to zero. Many such reparameterisations leave the

network functionally identical; yet couple to the optimisation in non-trivial ways. This introduces a mode to steer the training of such networks by explicitly breaking symmetry through the chosen reparameterisations/initialisation. Considering the map of Eqn. 31, representing a two-layer MLP with a diagonalised first layer and isotropic activation $\mathbf{f}(\vec{x}) = \bar{\sigma}(\vec{x}^T \vec{x}) \vec{x}$.

$$\vec{y}_i = \mathbf{W}_{ij} [\mathbf{f}(\vec{z})]_j + \bar{b}_i^{(2)} \quad \vec{z}_j = \bar{\Lambda}_j \vec{x}_j + \bar{b}_j^{(1)} \quad (31)$$

Computing the gradients of \mathbf{W} and $\bar{\Lambda}$ yields Eqn. 32.

$$\frac{\partial \mathcal{L}}{\partial \mathbf{W}_{pq}} = \bar{g}_p [\mathbf{f}(\vec{z})]_q \quad \frac{\partial \mathcal{L}}{\partial \bar{\Lambda}_p} = \bar{g}_i \mathbf{W}_{ij} \mathbf{J}_{jp}^{\mathbf{f}} \vec{x}_p \quad \frac{\partial \mathcal{L}}{\partial \bar{b}_p^{(1)}} = \bar{g}_i \mathbf{W}_{ij} \mathbf{J}_{jp}^{\mathbf{f}} \quad (32)$$

$$\mathbf{J}_{jp}^{\mathbf{f}}(\vec{z}) = \bar{\sigma}(\vec{z}^T \vec{z}) \delta_{jp} + 2\bar{\sigma}'(\vec{z}^T \vec{z}) \vec{z}_j \vec{z}_p$$

Since these null-like reparameterisations emerge as a singular value tends to zero, $\bar{\Lambda}_0 \rightarrow 0$ with bias $\bar{b}_0^{(1)} \rightarrow 0$, then as a consequence $\vec{z}_0 \rightarrow 0$ and $[\mathbf{f}(\vec{z})]_0 \rightarrow 0$ and from this a function-invariant reparameterisation $\mathbf{W}_{i0} = \vec{0}$ is admitted. By numerical substitution into Eqn. 32, one can determine that such a reparameterisation not only couples with the optimiser but produces a zero-valued fixed point for both \mathbf{W}_{i0} and $\bar{\Lambda}_0$ — stalling training. Hence, careful consideration of such null-like reparameterisations is essential, especially for neurogenesis initialisations, and an explicit symmetry breaking of $\mathbf{W}_{i0} \in \mathbb{R}^n \setminus \{\vec{0}\}$ is necessary, though it will bias the optimisation trajectory accordingly by any non-zero choice. Hence, a ‘no-free-lunch’ result arises; one must bias the behaviour of the network’s new neuron through a choice of $\vec{W}^* \neq \vec{0}$ or $b^* \neq 0$. To name several approaches, one may choose $\vec{W}^* \neq \vec{0}$ randomly, or a vector in the existing column-vector span of \mathbf{W} , or create a signed-bias in b^* or take it to equal the current intrinsic length, $b^* = \pm\sqrt{o}$ — many valid initialisations can help avoid this vanishing gradient problem, all with optimisation consequences.

B Considerations of Normalisation

Within isotropic multilayer perceptrons, one may wish to implement a form of normalisation, especially post-composed with the activation function, to mitigate activations growing and compensate for small singular values affecting the negligible impact assumption as $\Lambda_{ii} \rightarrow 0$. The usage of isotropic-tanh, $\sigma(a) = \tanh a$, similarly mitigates this with its saturation to 1. However, BatchNorm [42], LayerNorm [43], among others, do not exhibit standard orthogonal algebraic (Eqn. 1) equivariance re-individuating neurons despite isotropic activation functions. RMSNorm [44] does display such orthogonal equivariance, but pre- and post-composition with an isotropic activation presents difficulties due to a constant vector norm.

This is displayed in Eqn. 33 and Eqn. 34, for pre- and post-composition of L_2 -Norm (scaled RMSnorm), denoted as $\mathbf{N}(\vec{x}) = \vec{x} / \|\vec{x}\|_2$ (neglecting ε) and generic isotropic activation function, $\mathbf{f} = \bar{\sigma}(\vec{x}^T \vec{x}) \vec{x}$, for $\bar{\sigma} : \mathbb{R}^+ \rightarrow \mathbb{R}^+$ and constant $C \in \mathbb{R}$. This section assumes parameterless normalisers with a generally neglected, negligible ε for notational simplicity.

$$\mathbf{f}(\mathbf{N}(\vec{x})) = \bar{\sigma}(\hat{x}^T \hat{x}) \hat{x} = \bar{\sigma}(1) \hat{x} = C \hat{x} = C \mathbf{N}(\vec{x}) \quad (33)$$

$$\mathbf{N}(\mathbf{f}(\vec{x})) = \frac{\bar{\sigma}(\vec{x}^T \vec{x}) \vec{x}}{\|\bar{\sigma}(\vec{x}^T \vec{x}) \vec{x}\|_2} = \frac{\bar{\sigma}(\vec{x}^T \vec{x}) \vec{x}}{|\bar{\sigma}(\vec{x}^T \vec{x})| \|\vec{x}\|_2} = \frac{\vec{x}}{\|\vec{x}\|_2} = \hat{x} = \mathbf{N}(\vec{x}) \quad (34)$$

Consequently, $\mathbf{N} \circ \mathbf{f} = \mathbf{N}$, $\mathbf{f} \circ \mathbf{N} = C \mathbf{N}$, alongside \mathbf{N} ’s idempotence $\mathbf{N} \circ \mathbf{N} = \mathbf{N}$. Thus, alternative radial normalisation, such as reintroducing batch statistics, is encouraged when implementing normalisation with adaptive isotropic networks. This is described in Eqn. 35, which acts like RMSNorm/ L_2 -Norm using a batched estimate of the mean norm, $\mathbb{E}_{j \in B} [\|\vec{x}_j\|_2]$ and samples \vec{x}_i .

$$N_b(\{\vec{x}_i\}) = \frac{\vec{x}_i}{\mathbb{E}_{j \in B} [\|\vec{x}_j\|_2]} \quad (35)$$

Similarly, ‘FrobNorm’ over a matrix of batched samples $\mathbf{X} \in \mathbb{R}^{n \times b}$, using a Frobenius norm $\|\cdot\|_F$ could be used to similar effect, shown in Eqn. 36, with specific instance for RMSNorm comparability.

$$N_f(\mathbf{X}) \propto \frac{\mathbf{X}}{\|\mathbf{X}\|_F} \quad \left(\text{e.g.} = \frac{\mathbf{X}}{(b\sqrt{n})^{-1} \|\mathbf{X}\|_F} \right) \quad (36)$$

LayerNorm, $\text{LN} : \mathbb{R}^n \rightarrow \mathbb{R}^n$, does exhibit an equivariance to $O(n-1)$, with a $\varrho : g \rightarrow \text{GL}_n(\mathbb{R})$ representation which leaves $\vec{1}$ fixed: $\{\varrho'(g) | g \in O(n), \varrho'(g)' \vec{1} = \vec{1}\} \cong \{\varrho(g) | g \in O(n-1)\}$. In general, this ordinarily prohibits the usage of SVD diagonalisation, which necessitates a full $O(n)$ equivariance; however if one generalises the form of LayerNorm to parameterise mean as instead a weighted-mean, then an equivariance to $O(n)$ is restored through a direct-sum. This generalised form is displayed in Eqn. 37, $\text{LN}_{\hat{n}} : \mathbb{R}^n \times \mathbb{R}^n \rightarrow \mathbb{R}^n$, with equivariance displayed in Eqn. 38 for standard representation, notated in shorthand as $\forall \mathbf{R} \in O(n)$. A further Eqn. 1 prescription for normalisers.

$$\text{LN}_{\hat{n}}(\vec{x}; \hat{n}) = \frac{\vec{x} - \hat{n} \hat{n}^T \vec{x}}{\|\vec{x} - \hat{n} \hat{n}^T \vec{x}\|_2} \quad (37)$$

$$\text{LN}_{\mathbf{R}\hat{n}}(\mathbf{R}\vec{x}; \mathbf{R}\hat{n}) = \mathbf{R} \text{LN}_{\hat{n}}(\vec{x}; \hat{n}) \quad (38)$$

Thus, considering Eqn. 38, one may use LayerNorm in the neuroadaptive isotropic multilayer perceptron, given that the weighted mean is transformed as Eqn. 38 with the orthogonal basis change.

Similar generalisations may be considered to reinterpret BatchNorm, which typically exhibits standard permutation equivariance. In this formula, each vector element is divided by its standard deviation across the batch, with this element-wise approximation to full covariance-whitening inducing permutation equivariance — analogous to the second-moment elementwise approximation of the ADAM optimiser [40]. However, considering weights are closed under orthogonal transformations even for elementwise activations, thus training may explore such rotated representations; consequently, the reference basis through which diagonal (elementwise) variance is calculated may shift with training. Thus, one may consider BatchNorm as a batch-estimation of the diagonal of the full covariance matrix. The full covariance matrix transforms as a rank-2 tensor $\mathbf{C}' = \mathbf{R}\mathbf{C}\mathbf{R}^T$, with its diagonal approximatly transforming as $\vec{C}' = (\mathbf{R} \odot \mathbf{R}) \vec{C}$ for hadamard product \odot , as previously derived in Eqn. 27. These approximate transformations may be reasonable for three reasons: first, training may induce comparable rotations of the representation regardless; second, BatchNorm already relies on noisy batch-level estimates, so the approximate transformation may not introduce qualitatively different noise during training; and third, transformation to running statistics need not be undertaken during training, since each forward pass recomputes the relevant diagonal batch statistics in the current basis.

Thus, one may argue that since training time evolution will likely continuously rotate the basis in which the covariance is diagonally approximated anyway, at least until the weights stabilise, then this may justify an explicit basis transform used in the diagonalisation too. Hence, this treats BatchNorm with an approximate $O(n)$ equivariance, rather than permutation S_n equivariance only — especially during training time.

Similarly, one may periodically take the post-activation function vectors over a chosen set of inputs and determine the true covariance. Singular value decomposition of this symmetric matrix yields orthogonal matrices, which, in an isotropic network, can then act on the weights to produce representations in a new basis. In this basis, BatchNorm no longer produces a diagonal approximation to the whitening transform, but the exact whitening transform in reference to the chosen set due to the diagonalised covariance matrix. This is maintained at least until further training. At late training/inference time, this may be more problematic due to weights that have settled into a consistent basis for the diagonalised covariance, which downstream parameters may have specialised to. Therefore, it is proposed that regularly reparameterising weights to diagonalise the covariance during training may mitigate the risk of downstream parameters specialising on a specific approximation.

At inference time, the estimated statistics must also be transformed appropriately, with mean, $\vec{\mu}$, transforming as a rank-1 quantity $\vec{\mu}' = \mathbf{R}\vec{\mu}$ and standard deviation, $\vec{\sigma}$ as a diagonal rank-2 approximation $\vec{\sigma}' \odot \vec{\sigma}' = (\mathbf{R} \odot \mathbf{R}) (\vec{\sigma} \odot \vec{\sigma})$, then taking the elementwise square-root to recover $\vec{\sigma}'$ — or recompute this diagonal from scratch as a stored statistic. If one wishes to undertake this with neuroadaptation, then SVD weight-diagonalisation and adaptation must precede the transform that diagonalises the covariance matrix. This treatment of BatchNorm not as elementwise standardisation with permutation equivariance, but as diagonally approximated full-whitening with approximate orthogonal equivariance, is important for enabling the latter independent component analysis approach on pre-whitened vectors, as detailed further in *App. E* — especially in tandem with a network which is regularly reparameterised to produce layerwise diagonalised covariance during training to prevent basis-specialisation.

C Parallellising Matrix-Vector Products and Nested Functional Classes

Generalising isotropic multilayer perceptrons yields an asymptotic nested functional class, much like residual networks, but arising from the functional form permitted by the chosen orthogonal symmetry. This is given by all possible isotropic networks of depth d being notated as set \mathcal{F}_d such that $\mathcal{F}_d \subseteq \mathcal{F}_{d+1}$. This structure may be significant, offering an alternative to classical residual [45] connections, with an architectural constraint to maintain or monotonically increase width with depth, and a saturating isotropic function. Moreover, this approach clarifies a crucial decomposition showing that all matrix-vector computations can be parallelised up front for isotropic multilayer perceptrons.

Considering the two-layer isotropic affine map provided by Eqn. 39 and then re-expressing this equation using notation $\mathbf{f} = \bar{\sigma}(\|\bar{x}\|_2^2)\bar{x}$ for preactivation \bar{x} .

$$\bar{x}^{(d+1)} = \mathbf{W}^{(d+1)} \mathbf{f} \left(\underbrace{\mathbf{W}^{(d)} \mathbf{f} \left(\bar{x}^{(d-1)} \right) + \bar{b}^{(d)}}_{\bar{x}^{(d)}} \right) + \bar{b}^{(d+1)} \quad (39)$$

$$\bar{x}^{(d+1)} = \bar{\sigma} \left(\|\bar{x}^{(d)}\|_2^2 \right) \mathbf{W}^{(d+1)} \bar{x}^{(d)} + \bar{b}^{(d+1)} \quad (40)$$

Then expanding this recurrence relation, yields Eqn. 41 for two layers, for new contracted variables \mathbf{W}' and $\bar{b}'^{(d)'}$.

$$\bar{x}^{(d+1)} = \bar{\sigma} \left(\|\bar{x}^{(d)}\|_2^2 \right) \bar{\sigma} \left(\|\bar{x}^{(d-1)}\|_2^2 \right) \underbrace{\mathbf{W}^{(d+1)} \mathbf{W}^{(d)}}_{=\mathbf{W}^{(d+1)'}} \bar{x}^{(d-1)} + \bar{\sigma} \left(\|\bar{x}^{(d)}\|_2^2 \right) \underbrace{\mathbf{W}^{(d+1)} \bar{b}^{(d)}}_{=\bar{b}'^{(d)'}} + \bar{b}^{(d+1)} \quad (41)$$

Which can subsequently be generalised again for d -layer isotropic perceptron, as shown in Eqn. 42. For notational simplicity a further reparameterisation to $\mathbf{W}_\circ^{(d)}$ and $\bar{b}_\circ^{(d,i)}$ is utilised. The input $\bar{x}^{(0)}$ does not undergo \mathbf{f} 's non-linear transform due to it being the input, hence indexing starts at 1.

$$\bar{x}^{(d+1)} = \bar{b}^{(d+1)} + S_1^d \mathbf{W}_\circ^{(d)} \bar{x}^{(0)} + \sum_{i=1}^d S_i^d \bar{b}_\circ^{(i,d)} \quad S_m^d = \prod_{j=m}^d \bar{\sigma} \left(\|\bar{x}^{(j)}\|_2^2 \right) \quad (42)$$

In this case, the layerwise architecture still matters for the $\bar{\sigma}$ terms, with the directionality of intermediate \bar{x} also affecting the various non-linear terms. This reparameterisation generally constrains the parameters $\mathbf{W}_\circ^{(d)}$ and $\bar{b}_\circ^{(i,d)}$; however, it is suggested to broaden the functional class by allowing both to be new, trainable, real matrices of appropriate shape. Hence, instead of interdependence between $\mathbf{W}_\circ^{(d)}$ depthwise, they are now treated as independent parameters, enabling up to full rank matrices, not limited to being less than or equal to the minimum rank of the original matrices in the contraction — the independent formulations are not subject to constraint $\text{rank} \left(\mathbf{W}_\circ^{(d)} \right) \leq \min_k \text{rank} \left(\mathbf{W}^{(k)} \right)$. Thus, unconstraining to general real matrices broadens the functional class and also enables further parallelisation at training time instead of requiring an initial sequential contraction of the intermediate weight matrices. They may also be trained as independent weight matrices.

Under the assumptions of a maintained or monotonically increasing width, with a non-linear term of an isotropic activation function, $\bar{\sigma}$, capable of saturating to a non-zero constant, with intrinsic length parameter able to ensure such general saturation — then in this saturation limit, the parameters of layer $d+1$ are able to embed the parameters of layer d , thus reproducing its function in that embedded (sub)space. In the uncontracted parameters, this is equivalent to a multiplication by a scaled identity, where the scaling is the inverse of the constant-saturated value of the non-linearity, which now acts as a constant linear scaling. Thus, given this architectural arrangement and asymptotic saturation limit, increasing depth retains the expressibility of all shallower networks while exhibiting a strictly equal-to-enlarged function class.

Furthermore, one may note that by this construction, *all* matrix-vector products, over all layers, $\bar{z}^{(d)} = \mathbf{W}_\circ^{(d)} \bar{x}^{(0)}$, may be precomputed *in parallel* by producing the $\bar{z}^{(d)}$ contraction. This is displayed

in Eqn. 43, showing sequential computation only need occur for inner products, $a = \vec{x}^{(d)} \cdot \vec{x}^{(d)}$ in $\mathcal{O}(n)$ per-layer-scaling for n width, a single non-linear operation, $\bar{\sigma}(a)$ in $\mathcal{O}(1)$ (compared to elementwise $\mathcal{O}(n)$ per-layer-scaling), scalar-vector product $\mathcal{O}(n)$ and vector-vector addition, $\mathcal{O}(n)$. This remains valid for the general $\mathbf{W}_o^{(d)}$ or $\vec{b}_o^{(i,d)}$ the original constrained forms: $\mathbf{W}_o^{(d)} = \prod_{i=1}^{d+1} \mathbf{W}^{(i)}$ and $\vec{b}_o^{(i,d)} = \left(\prod_{k=i+1}^{d+1} \mathbf{W}^{(k)} \right) \vec{b}^{(i)}$.

$$\vec{x}^{(d+1)} = \vec{b}^{(d+1)} + S_1^d \vec{z}^{(d)} + \sum_{i=1}^d S_i^d \vec{b}_o^{(i,d)} \quad (43)$$

Hence, the computationally demanding matrix–vector products are *all* parallelised and precomputed, whilst comparatively trivial scalar-vector, inner products, vector additions and simple $\mathcal{O}(1)$ activations are sequential, potentially offering significantly improved GPU utilisation.

D Sketching Adaptive-Channel Convolutional Networks

The procedure for isotropic-adaptive networks can be generalised for convolutional networks. This section sketches such results and will be developed in future work.

A dynamical convolution architecture is enabled by implementing isotropic activation functions, \mathbf{f} , channel-wise — taking the norm over vectors in \mathbf{R}^C for C channels. In analogy to the multilayer perceptron setup, a partial diagonalisation of each convolution’s kernel parameters, $\mathbf{K}_1 \in \mathbb{R}^{C_{\text{out}} \times (C_{\text{in}} \times K_h \times K_w)}$, is possible as shown by Eqns. 44 through 47, for $\mathbf{R} \in \mathcal{O}(C_{\text{out}})$, $\mathbf{Q} \in \mathcal{O}(C_{\text{in}} K_h K_w)$ and diagonal $\mathbf{\Lambda}$.

$$\mathbf{Y} = \mathbf{K}_2 * \mathbf{f} \left(\mathbf{K}_1 * \mathbf{X} + \vec{b}_1 \right) + \vec{b}_2 \quad (44)$$

$$\mathbf{Y} = \mathbf{K}_2 * \mathbf{f} \left((\mathbf{R} \mathbf{\Lambda} \mathbf{Q}^T) * \mathbf{X} + \vec{b}_1 \right) + \vec{b}_2 \quad (45)$$

$$\mathbf{Y} = \underbrace{\mathbf{K}_2 \mathbf{R}}_{=\mathbf{K}'_2} * \mathbf{f} \left(\underbrace{\mathbf{\Lambda} \mathbf{Q}^T}_{=\mathbf{K}'_1} * \mathbf{X} + \underbrace{\mathbf{R}^T \vec{b}_1}_{=\vec{b}'_1} \right) + \vec{b}_2 \quad (46)$$

$$\mathbf{Y} = \mathbf{K}'_2 * \mathbf{f} \left(\mathbf{K}'_1 * \mathbf{X} + \vec{b}'_1 \right) + \vec{b}_2 \quad (47)$$

In effect, the spatial indices of convolution must be kept consistent, but rotations can commute with isotropic functions, thereby partially diagonalising channels and enabling the described adaptation. Generalising the approach is non-trivial when considering both padding and residual constructions, requiring substantial further development; yet this notated approach presents a route to broader generalisation. Similarly, such a fully diagonalised, partially diagonalised or ICA-based approach may offer interpretable insights into representations, with the caveat that representations may change under isotropic functions [25].

E Independent Component Analysis (ICA) Network Representation

Independent component analysis (ICA) is a standard statistical technique for linearly separating a mixture of signals into often meaningful, statistically independent channels for interpretation — typically relying on non-Gaussianity for separation. This could be used for interpretable isotropic networks at inference time, up to the inherent concept resolvability of ICA itself for hidden-layer representations. Given interpretable components produced by ICA, one may monitor the activation elements to determine a network’s current expression of internal concepts.

This approach may be utilised only on the premise that the multilayer perceptron is constructed from sequential blocks of affine-map \rightarrow isotropic activation function \rightarrow BatchNorm — in a covariance-eigenbasis representation, thus diagonalising the post-activation function’s covariance. The network should also be trained such that it is not contingent on any particular basis inherited from BatchNorm’s diagonal-covariance approximation but largely invariant to orthogonal transforms of the affine layers

(discussed in the BatchNorm section of *App. B*). Thus, this ensures a pre-whitened signal ready for the subsequent ICA step.

One may then use various approaches to determine the orthogonal matrix required by ICA to transform the whitened data — such as a loss that encourages non-gaussianity and optimising in the corresponding $\mathfrak{so}(n)$ Lie algebra space. Having determined the appropriate orthogonal transform, \mathbf{Q} , one may reparameterise the network in one of three distinct approaches, given that an identity is postcomposed with BatchNorm I = $\mathbf{Q}^T \mathbf{Q}$ and that the \mathbf{Q}^T matrix is used to reparameterise the subsequent affine-layer weights: $\mathbf{W}'_{(n+1)} = \mathbf{W}_{(n+1)} \mathbf{Q}^T$. These proceed identically in algebra to the partial-diagonalisation insertion of an identity, but with a different pair of rotations and corrections to BatchNorm’s statistics, detailed below. Transforms are detailed in *Eqns. 48 through 52*, for parameterless BatchNorm, $BN(\vec{x}; \vec{\mu}, \vec{C})$ and isotropic activation function \mathbf{f} .

$$\vec{x}_{(n+1)} = \mathbf{W}_{(n+1)} \vec{z}_{\text{whi.}} + \vec{b}_{(n+1)} \quad \vec{z}_{\text{whi.}} = \text{BN} \left(\mathbf{f} \left(\mathbf{W}_{(n)} \vec{x}_{(n)} + \vec{b}_{(n)} \right); \vec{\mu}, \vec{C} \right) \quad (48)$$

$$\vec{x}_{(n+1)} = \mathbf{W}_{(n+1)} \underbrace{\left(\mathbf{Q}^T \mathbf{Q} \right)}_{=I} \vec{z}_{\text{whi.}} + \vec{b}_{(n+1)} \quad \vec{z}_{\text{whi.}} = \text{BN} \left(\mathbf{f} \left(\mathbf{W}_{(n)} \vec{x}_{(n)} + \vec{b}_{(n)} \right); \vec{\mu}, \vec{C} \right) \quad (49)$$

$$\vec{x}_{(n+1)} = \underbrace{\mathbf{W}_{(n+1)} \mathbf{Q}^T}_{=\mathbf{W}'_{(n+1)}} \underbrace{\mathbf{Q} \vec{z}_{\text{whi.}}}_{=\vec{z}_{\text{ICA}}} + \vec{b}_{(n+1)} \quad \vec{z}_{\text{whi.}} = \text{BN} \left(\mathbf{f} \left(\mathbf{W}_{(n)} \vec{x}_{(n)} + \vec{b}_{(n)} \right); \vec{\mu}, \vec{C} \right) \quad (50)$$

$$\vec{x}_{(n+1)} = \mathbf{W}'_{(n+1)} \vec{z}_{\text{ICA}} + \vec{b}_{(n+1)} \quad \vec{z}_{\text{ICA}} = \text{BN} \left(\mathbf{f} \left(\underbrace{\mathbf{Q} \left(\mathbf{W}_{(n)} \vec{x}_{(n)} + \vec{b}_{(n)} \right)}_{=\mathbf{W}'_{(n)} \vec{x}_{(n)} + \vec{b}'_{(n)}} \right); \vec{\mu}', \vec{C}' \text{ or } \mathbf{C}' \right) \quad (51)$$

$$\vec{x}_{(n+1)} = \mathbf{W}'_{(n+1)} \vec{z}_{\text{ICA}} + \vec{b}_{(n+1)} \quad \vec{z}_{\text{ICA}} = \text{BN} \left(\mathbf{f} \left(\mathbf{W}'_{(n)} \vec{x}_{(n)} + \vec{b}'_{(n)} \right); \vec{\mu}', \vec{C}' \text{ or } \mathbf{C}' \right) \quad (52)$$

From this point, there is an explicit \mathbf{Q} matrix product retained, which may remain as is, necessitating an additional matrix-vector product per sample, or absorbed into prior parameters to increase efficiency. These latter reparameterisation approaches temporarily assume the orthogonal equivariance of the full-whitening and isotropic activation function, commuting with \mathbf{Q} such that \mathbf{Q} may be absorbed into preceding affine-layer’s weights, $\mathbf{W}'_{(n)} = \mathbf{Q} \mathbf{W}_{(n)}$, and biases $\vec{b}'_{(n)} = \mathbf{Q} \vec{b}_{(n)}$. Assumed to be in a static covariance-diagonalised representation ready for inference-time, one may then choose to appropriately transform the mean, $\vec{\mu}' = \mathbf{Q} \vec{\mu}$, and covariance matrices $\mathbf{C}' = \mathbf{Q} \mathbf{C} \mathbf{Q}^T$, necessitating a matrix-vector product per sample rather than the diagonalised vector-vector Hadamard product (exact). Alternatively, one may choose to retain the efficient vector-vector product nature of BatchNorm by approximating the original function with a diagonal-approximated covariance $\vec{C}' = (\mathbf{Q} \odot \mathbf{Q})^T \vec{C}$ (inexact). Either of the latter two methods appears preferable to the first exact approach, which introduces a needless additional matrix-vector product.

Table 3: Two primary approaches for a network in the ‘ICA-representation’ with respective trade-offs.

Variant	Functional Invariance	Computational Cost
\mathbf{Q} absorbed with full covariance	Exact, under assumptions	Loses diagonal BatchNorm efficiency
\mathbf{Q} absorbed with diagonal covariance	Approximate	Retains BatchNorm’s efficiency

In both exact cases, the ‘neurons’ associated with the vectors decomposed in the standard basis now represent independent components as specified by ICA and can be interpreted accordingly. The inexact approach approximates such components given the BatchNorm diagonal preweighting approximation. Thus, this ICA representation of the network may enable real-time monitoring of the network’s hidden states and interpretability therein, at least up to the inherent concept resolvability of ICA.

Alongside diagonalising via singular value decomposition, this approach may enhance interpretability but does not concurrently permit sparsification for more efficient computation and memory, unless in the exceedingly unlikely circumstance where both transforms coincide. Thus, this introduces an interpretability-sparsification tradeoff within isotropic networks — yet both retain the isotropic MLP

‘big- \mathcal{O} ’ scalings detailed in *App. C* which may be preferable to standard MLP’s scalings. Corresponding approaches may also apply to the sketched convolutional form of *App. D* for interpretability. Unlike sparsification, which may only be enacted for every other layer, the ‘ICA-representation’ of the network can be introduced for every hidden-layer map.

Overall, this demonstrates the flexibility of standard-orthogonal prescribed primitives, beyond neuroadaptation.

F Notation

- $\mathbb{R}_{\geq 0}$: Non-negative real numbers.
- \mathbb{Z}_+ : Positive integers.
- \vec{a} : Vectors. \mathbf{A} : Matrices.
- \circ : Function composition.
- \odot : Hadamard, or elementwise, product.
- $\|\vec{x}\|_2$: Euclidean norm of \vec{x} .
- \hat{x} : Unit-normalised vector $\hat{x} = \vec{x}/\|\vec{x}\|_2$.
- \hat{e}_i : i th standard basis vector.
- δ_{ij} : Kronecker delta.
- \mathbf{I}_n or \mathbf{I} : Identity matrix.
- $\text{diag}(\mathbf{A})$: Vector formed from the diagonal entries of matrix \mathbf{A} .
- $\text{diag}^\dagger(\vec{v})$: Diagonal matrix whose diagonal entries are the components of \vec{v} .
- \mathbb{P} : Probability measure.
- $\mathcal{O}(\cdot)$: Big- \mathcal{O} notation.
- \mathcal{G} : Group and $g \in \mathcal{G}$: an element of that group.
- $\varrho^{(1)}(g), \varrho^{(2)}(g), \varrho(g)$: Different group representations.
- $O(n)$: Orthogonal group in dimension n .
- $\text{GL}_n(\mathbb{R})$: General linear group of invertible $n \times n$ real matrices.
- S_n : Permutation group on n elements.
- \mathbf{P}_π : Matrix representation of permutation π .
- $P = \{\varrho(\pi) \mid \pi \in S_n\}$: Set of all permutations in the group in a chosen matrix representation.
- $O = \{\varrho(Q) \mid Q \in O(n)\}$: Set of all elements in the orthogonal group in a chosen matrix representation.
- $[\mathbf{R}, \mathbf{f}]$: Commutator $\mathbf{R} \circ \mathbf{f} - \mathbf{f} \circ \mathbf{R}$.
- \mathcal{F} : Functional class.
- \mathcal{F}_d : Functional class of isotropic networks of depth d .
- f, \mathbf{f} : Function, emboldened notation is a vector-valued function.
- $f_{\text{Aff.}}$: Affine map.
- $f_{\text{Iso.}}$: Isotropic activation function.
- σ : Scalar nonlinearity used to construct an isotropic activation, with alternative formulations $\tilde{\sigma}, \bar{\sigma}$ defined by *Eqns. 5*.
- $J_{\mathbf{f}}$: Jacobian of function \mathbf{f} .
- $\mathbf{N}(\vec{x})$: Parameterless L_2 normalisation map, $\mathbf{N}(\vec{x}) = \vec{x}/\|\vec{x}\|_2$.
- LN: LayerNorm.
- BN: BatchNorm.
- $\mathbf{\Lambda}$: Diagonal or rectangular diagonal matrix of singular values.
- ϑ : Singular-value threshold.
- Ξ : Desired number of scaffold neurons to maintain below threshold.
- ω : Current number of scaffold neurons, defined by singular values below ϑ .
- o : Intrinsic length parameter introduced for neuroadaptation.
- b_* : Bias component associated with an appended or deleted neuron/channel.
- \vec{W}_* : Appended or deleted downstream weight column associated with a scaffold neuron/channel.
- $\vec{\psi}$: Compensatory vector parameter used to absorb additive terms arising during pruning.
- ϵ : Mean per-example L_2 discrepancy between logits or activations before and after adaptation or sparsification.
- ϵ : Small positive stabilisation constant in normalisers.
- Σ_0 : Mean initial sum of singular values in Experiment One.
- Σ_1 : Sum of singular values after neuroadaptation in Experiment One.
- θ : Generic model parameter; also used when counting non-zero parameters.
- \mathcal{L} : Loss function. $\nabla_{\vec{a}}\mathcal{L}$: Gradient of the loss with respect to parameter vector \vec{a} .
- η : Learning rate.
- $\mathbf{R}^{\odot 2} = \mathbf{R} \odot \mathbf{R}$: Shorthand for elementwise square of an orthogonal matrix. Generally $\mathbf{R}^{\odot n}$ for elementwise power.

G Limitations, Assumptions, and Applicability

The intention of this section is to clarify and discuss the known limitations of the approaches discussed — ranging from diagonalisation, architectural considerations and approximations.

Due to the nature of the diagonalising transforms, this approach requires two parameterised maps that exhibit closure invariance under standard orthogonal transforms on the respective sides. None or any number of interspaced standard orthogonal algebraic equivariant functions may be utilised. In practice, this likely necessitates a densely parameterised dimension for the orthogonal transform to act on, and a non-linear function that is orthogonal-equivariant. Isotropic multilayer perceptrons are straightforward networks that exhibit such properties, with a potential generalisation to convolutional networks described in *App. D*. However, other state-of-the-art networks, such as transformers [34], do not exhibit this relation, necessitating future work to determine whether the architectural constraints can be broadened beyond MLP networks. Some residual networks can be redesigned to exhibit this property, but diagonalisation introduces complications, as all residually connected layers must be transformable simultaneously. Nevertheless, MLP architectures remain pertinent in applications with unknown inductive biases, preventing the specialisation of the architecture class. They are also widely used as backbone subcomponents in larger networks, including transformers, where such neuroadaptive techniques can be applied when two or more such layers occur sequentially.

Another consideration is that of the orthogonal-prescribed primitives in an MLP, and whether it retains the expressibility of typical construction with permutation-prescription. The construction of the adaptive topology is not contingent on any single isotropic activation function, but on the general form. Furthermore, the competitiveness of this form cannot be ascertained from any single function or application, since it represents a broad functional form whose inherent performance relative to elementwise formulae is currently unknown. Moreover, the chosen isotropic-tanh is merely a superficial analogue of standard tanh (itself not typically optimal), intended as a provisional placeholder that saturates below 1 to prevent the need for normalisations which introduce confounders. These functional forms do not appear comparable, particularly optimisation dynamics in *Figs. 4 and 5*, regardless of this superficial similarity. However, due to generality, the verification empirics did not require optimality; isotropic-tanh was sufficient to confirm the underlying mechanisms regardless. Nevertheless, the results of *App. I.6* are encouraging showing despite this placeholder, it typically outperforms standard-tanh for deeper and wider MLP architectures on more challenging visual-classification datasets.

Similarly unknown is any universal approximation theorem for such a form yet, which does not imply its absence either; whilst, the pragmatic usage of elementwise formulae proceeded for the intermediate 31 years between Rosenblatt’s canonical work [46] and Cybenko’s first universal approximation theorem [47], alongside their underappreciated specificity to particular architecture. Thus, such an unknown is not immediately discouraging; additionally, some precedent exists for incidental normed nonlinearities [48, 25] with motivation outside of a symmetry-prescription formalism (not to be confused with radial-basis functions [49]). Regardless, in the worst-case scenario, the newly enabled behaviours may, in several circumstances, outweigh mild accuracy suboptimality. If one wishes to optimise for competitiveness or production, a substantial search over isotropic functions should be undertaken; this remains a limitation for future research, given that the underlying mechanisms are now substantiated.

This also relates to the weight-parameterisations and redundancies therein. Under the standard permutation-prescription, the unique weight-space is $\mathbb{R}^{n \times m} / S_n$ in shorthand, with a generic group size of $|S_n| = n!$ multiplying the functionally distinguishable parameterisations. Further reduction occurs for hyperoctahedral-prescribed activation functions to $\mathbb{R}^{n \times m} / B_n$, in shorthand, with group size $|B_n| = 2^n n!$ multiplying unique parameterisations³. Whether this retains expressibility, given increasingly redundant parameterisations, remains unclear. Orthogonal-prescribed multilayer perceptrons further reduce the number of effective, unique parameters, as they are a supergroup, $S_n \subset B_n \subset O(n)$, yielding a continuous orbit of reparameterisations. They may be more intuitively parameterised as the partial-diagonal representations for all but the final layer $\mathbf{R}\mathbf{A} \in \mathbb{R}^{n \times m}$, where \mathbf{R} has degrees of freedom $0.5n(n-1)$ from its Lie-algebra parameterisation, and magnitude ordered \mathbf{A} with $\min(n, m)$ degrees of freedom. Whether these degeneracies and reduced unique parame-

³These should not be confused with the two-sided closures B_n , B_m , or S_n , S_m or $O(n)$, $O(m)$ also applicable, but would reduce parameterisation for every other layer, instead one-side closures are detailed which are relevant for every layer except the output.

terisations are harmful or helpful for expressibility is presently unclear. Such considerations may, reductionistically, come down to whether better minima emerge along what would be the orthogonal orbit for the subgroups S_n and B_n , with potentially *usefully* nuanced loss structure arising due to the absence of continuous redundancy, whereas such minima wouldn't arise for the flattened-loss orbits induced by orthogonal-group prescriptions. Conversely, such local minima could be troublesome for optimisation if unfavourable, whereas a flattened orbit may offer better learning efficiency by avoiding them, since it has a zero gradient, reducing exploration of the continuous orbit-flattened loss. This appears highly specific to the particularities of the seemingly non-comparable, non-linear relationship of the two functional forms. Some results do suggest a parameter-symmetry dependence on training phenomena[50].

A further limitation is that neurodegeneration is, in general, unavoidably approximate in its function invariance. This is because, unlike neurogenesis, one cannot *generally* embed the original parameters, $\text{rank}(\mathbf{W}') \leq \text{rank}(\mathbf{W})$. However, this motivated several compensatory parameters, the intrinsic length and psi-vector, which were shown (Tab. 1) to improve the approximate invariance considerably compared to their absence — although this induces an ordering from final to first layer neuroadaptation to ensure psi-vector compensation only propagates to one subsequent layer. For the same reason, this psi-vector parameter should be decayed prior to the next neuroadaptation, and this may also help mitigate any non-linear instability in its action (although by Tab. 4 this appears inconsequential).

Furthermore, with the use of a saturating isotropic activation function, or with the discussed normalisation, activation magnitudes cannot grow to compensate for a decaying singular value — thus, reliably implying that such singular values do have a low impact on overall model functionality. Hence, despite the inherent limitations and function invariance during neurodegeneration, the methodology presented does take several steps to mitigate this function drift — confirmed then empirically in Tab. 1 results.

Similarly, the results of App. A.3 implies that neurogenesis initialisation should not be zero in \vec{W}^* due to inducing an optimisation fixed-point, and $b^* = 0$ is a necessity to ensure true function invariance, as otherwise the subsequent biases would need a non-linear correction. This produces a chosen explicit symmetry breaking at initialisation, biasing the network along a particular optimisation trajectory. As discussed, these choices of explicit symmetry-breaking initialisations may be explored to achieve various effects. Neither is explicit symmetry breaking inherently problematic, as evidenced by the many initialisers in standard use.

It is also essential to clarify that several claims are true only asymptotically; for example, the sparsification result is highly architecture-specific, with the stated formulae valid only for constant-width isotropic multilayer perceptrons. Similarly, the case is for isotropic nested functional classes, which is only valid for monotonically increasing width isotropic MLPs, in the regime where the final activation function becomes 'saturated' (constant in its non-linear term). Nevertheless, several isotropic functions, including isotropic-tanh, do display such saturating behaviour, particularly when considering the positive-definite intrinsic length, and considerable sparsification was demonstrated, Tab. 6, for finite width and depth architectures, consistent with Eqns. 55 and 56.

Other considerations, such as hyperparameter optimisation and SVD-scheduling, could be explored if one wished to demonstrate competitive performance beyond the validation of the theoretical claims prioritised in this paper. Additionally, the neuroadaptation of the architecture was shown to be negligible in terms of compute time compared to standard training and testing set evaluation, showing that the method's practical cost is dominated by the underlying model training rather than by the adaptation procedure itself. Thus, one may increase the frequency of neuroadaptation beyond once per epoch with little ramification on compute time.

Further limitations regarding diagonalisation approximations for rank-2 quantities, as used in existing optimisers and normalisers, can also affect invariance in the optimisation trajectory and forward-pass inference, respectively. However, they can be approximately transformed to explicitly compensate; moreover, the concern is mitigated by the likely rotationally degenerate parameterisations being explored regardless through training, with little impact observed thus far on such quantities.

Finally, the empirical component is intended as a mechanism verification rather than a competitive or SOTA-scale implementation. This reflects the paper's primarily theoretical-conceptual contribution: a symmetry-prescriptive ontology and a structural invariance mechanism. Using this foundation, orthogonal-prescribed primitives were utilised to admit orthogonal reparameterisations, enabling

various behaviours, including basis independence, SVD-based diagonalisation, sparsification and function-preserving neuroadaptation. These analytical results, therefore, require empirical verification first; the contribution lies primarily in the novel possibilities afforded by a symmetry-prescriptive ontology, rather than a focus on any single optimised experimental procedure. Alongside the restriction to multilayer perceptrons, limiting SOTA possibilities.

Accordingly, the experiments focus on invariance, adaptation dynamics, and computational overhead as the most direct, meaningful tests of the proposed mechanism. The experiments are therefore not presented as evidence of competitiveness but as controlled, minimalist tests of whether the proposed symmetry mechanism behaves as predicted, while minimising confounders of the mechanism. At this stage, large-scale benchmarks would introduce such confounders — architecture choice, activation-function optimality, optimiser interactions, normalisation, data augmentation, and engineering scale — hence, these minimal mechanism-verification experiments were preferred. Given the early stage of the proposed *general* symmetry-prescribed foundation, it would be inappropriate to expect competitive results against mature transformer or convolutional systems, which may themselves be predicated on different architectural and primitive choices. Initial results with placeholder activation functions should therefore be interpreted as verification of the mechanism, not as assessments of the broader functional class enabled by symmetry-prescribed primitives. Overall, establishing novel mechanistic possibilities upfront, before refining every component for competitive optimality, is preferable and enabled testing of the paper’s core claims. However, substantial future work is required to determine the exact pipeline optimisation, hyperparameter search and activation function selection needed for competitive SOTA comparisons.

H Related Works

The works of ‘Net2Net’ [51], particularly ‘Net2WiderNet’, and ‘Network Morphism’ [52], display some relation to this work in terms of neurogenesis considerations. These works effectively ascertain how to embed a narrower network architecture within a wider one whilst preserving function. The observation in the Net2WiderNet work is that for an elementwise activation function, one may arbitrarily duplicate an existing column vector to widen a layer’s weight matrix, shown in Eqn. 53 with $\vec{W}_{(1)} \in \text{column}(\mathbf{W}_{(1)})$, provided that the corresponding outgoing weights in the subsequent layer are divided among the duplicated units so that their sum equals the original outgoing weight, shown on the right of Eqn. 53 with $\vec{C}_{\text{duplicity}}$ being a vector correcting for duplicity. The appended vectors are functions of their corresponding weights: $\vec{W}_{(i)}^*(\mathbf{W}_{(i)})$.

$$\mathbf{W}'_{(1)} = \left(\mathbf{W}_{(1)}, \vec{W}_{(1)}^*(\mathbf{W}_{(1)}) \right) \quad \mathbf{W}'_{(2)} = \vec{C}_{\text{duplicity}} \odot \left(\vec{W}_{(2)}^*(\mathbf{W}_{(2)}) \right) \quad (53)$$

This is arguably a form of neurogenesis for elementwise activations that increases a layer’s neuron count, but is otherwise distinct from the singular-value approach enabled by isotropic formulations, discussed in this paper. As a result, there are considerably different embeddings, such as the SVD approach appending a zero column to the singular values and then makes an unconstrained choice in the corresponding row of the subsequent layer. This is achieved only by exploiting the reparameterisation symmetry prescriptively introduced into primitives for this purpose. Additionally, neurodegeneration is not covered by the Net2Net formulations, and neurogenesis requires some noise to break the optimisation symmetry and drive neural differentiation — this noise results in a small error in function preservation. The explicit symmetry breaking introduced in this paper is qualitatively different, preserving the function exactly via null-like reparameterisations whilst desirably breaking the optimiser’s symmetry. It would appear that near-zero noisy initialisations may also be possible within the Net2WiderNet framework. Network morphism addresses a problem similar to Net2Net’s, but within a more general framework using non-identity factorisations.

Overall, despite a common aim of increasing a network’s width, the stated approaches differ from those of this paper in that they approach function invariance through different methodologies. Further, the results of App. I suggests an incomparability of functional forms even for superficially similar non-linear terms, with Net2WiderNet contingent on elementwise formulae, and this work is centred on symmetry-led isotropic formulae. However, both formulations demonstrate function-invariance under neurogenesis.

Additionally, some techniques from Net2DeeperNet and Network Morphism may be combined with the present work by parameterising the isotropy $\mathbf{f}_*(\vec{x}; \alpha) = \alpha\vec{x} + (1 - \alpha)\mathbf{f}(\vec{x})$, $\alpha \in [0, 1]$ in order to insert new layers. Alternatively, one may exploit the local linearity about the origin $\mathbf{J}_{\mathbf{f}|_{\vec{0}}} \propto \mathbf{I}_{n \times n}$ of isotropic activation functions to similar effect, given a normalisation that guarantees the magnitudes will not enter a highly non-linear region of the activation function. Thus, overlap could be established through Net2DeeperNet.

Rigging-The-Lottery (RigL) [17] more clearly draws a distinction with the present work. Motivationally, RigL responds to the Lottery-Ticket hypothesis [53], which posits that a sparse network found through pruning can be matched or improved upon by training that sparse architecture alone from its original initialisation — RigL demonstrates the performance of a training-time sparsely adaptive network. Thus, Rigging-the-Lottery focuses on training networks with sparse representations from the start and progressively performing further connectivity pruning or re-enabling through learning, based on criteria such as growing based on dense-gradient comparisons and pruning based on weight magnitude. Thus, this is an example of adaptable connectivity rather than neuroadaptability introduced in this paper; the dense network’s width remains static. This connectivity pruning does change the directionality of the weight-matrix columns, unlike a singular-value thresholding-of-importance approach, which may be undesirable. Through such a singular-value approach, these pruned weight columns become single non-zero entries, and thus decay-or-removal does not affect directionality, whilst such an approach also makes connectivity pruning equivalent to full neurodegeneration. Furthermore, this paper’s diagonalised representation yields a significant $1 - \min(m^{-1}, n^{-1})$ connectivity sparsity for a single weight matrix with identically invariant function, which experiments could explore in terms of the lottery-ticket hypothesis.

Together with the Single-Shot Network Pruning (SNIP) [16] (also a connectivity-pruning technique), these papers also indicate an alternative thresholding approach, namely loss sensitivity, which could be similarly explored for this paper’s neurodegeneration pipeline.

Independent of the present work, neuron merging [19] provides a useful comparison on neurodegeneration. This approach uses a weight ‘factorisation/decomposition’, which retrospectively may be considered to leverage a scaled-permutation-described network. It does this for neurodegeneration by attempting to compensate for functional loss by merging the removed neuron’s contribution into a retained, similar neuron. Together, with a strong constraint of ReLU, it effectively utilises an (unstated) positive-scaled permutation (positive-monomial) equivariance exhibited by ReLU [22] to move such scalings through the activation function.

The decomposition leverages the interdependence among the weight column vectors to reexpress the removed (individuated) neurons as a scaling of a single remaining column vector (not a general linear combination), using cosine similarity for comparability. However, it is important to consider that this is not an algebraic weight-factorisation like SVD, it is an approximate nearest-retained-neuron compensation rule, presupposing the existence of column-wise redundancy for good approximation, rather than a spectral ranking of function contributions. Thus, a strong approximation enters earlier than the generally necessitated neurodegenerative approximation.

The singular-value structure also provides a potentially clearer proxy for the importance of (diagonalised-)neurons. When combined with bounded-norm activations, they indicate the functional impact of neurodegeneration. This contrasts with the cosine similarity and the separate pruning-criterion heuristics required by the individuated-neuron constraint, which are only roughly indicative of the neuron’s functional redundancy among existing neurons.

The isotropic constraint of this work is also a broad functional form constraint rather than a specific-instance constraint of elementwise-ReLU in the neuron merging paper. However, this may be generalised retrospectively to positive-monomial-prescribed primitives for this paper, with ReLU as the practical example. Overall, this approach has similarities but is explicitly limited to the elementwise-ReLU case and is restrictive in that removed weight columns must be approximately redundant, described near-collinearity with a preserved column vector. However, when combined with Net2WiderNet’s work on neurogenesis, one could consider that this combination enables a form of neuroadaptability in networks described by scaled permutation equivariance (ReLU multilayer perceptrons).

Overall, in many respects, the isotropic adaptive topologies enable both considerable connectivity pruning through sparsification and also full neurodegeneration. They enable arbitrarily well-

approximated function invariances for thresholded neuroadaptation by exploiting their symmetry-led design. Prior work recovers only aspects of this full regime, limited to one of neurogenesis, neurodegeneration or connectivity-sparsity, rather than a full integrated approach. Moreover, these prior works are limited by neuron individuation, a significant hurdle to network adaptation due to the high interconnectivity among individuated neurons, which is not present among diagonalised neurons. This paper’s approach to reformulating primitives through orthogonal, equivariant prescriptions to deindividuate neurons enables a broader use of decomposition tools, most notably singular-value decomposition, to construct function-invariant diagonalised representations. This yields a basis for treating connectivity sparsification, neurogenesis, and neurodegeneration (becomes equivalent to connectivity pruning) within a common framework, rather than as separate heuristic procedures.

Consequently, direct comparison with elementwise approaches is limited: they operate within the inherited symmetry structure of conventional neuron-indexed networks, whereas the present work alters the primitive symmetry class itself, making adaptive topology a consequence of the network’s reparameterisation structure — and incurring considerably different computational approaches, shown in *App. I.2*, further limiting comparison.

I Experimental Details

This section covers all experimental details used in the production of the plots and tables of *Sec. 3*. It also includes additional verification results, such as sparsification invariance and spectra evolution of standard-tanh networks. This paper primarily presents the theoretical developments underpinning such architectures, and the experiments are intended to substantiate those theoretical claims.

Generic hyperparameters were used across all experiments to ensure consistency and that observed effects were attributable to the general theoretical formulation rather than to carefully selected parameter settings. These hyperparameters are as follows: learning-rate $\eta = 1 \times 10^{-3}$, batch-size, $B_s = 48$, orthogonal initialisation, all networks are trained with ADAM-w [54] with L_2 weight decay, $\lambda = 1 \times 10^{-3}$ (otherwise PyTorch [55] defaults were used), additional psi-vector L_2 decay $\lambda_{\psi} = 0.1$ (due to the fast decay to zero being an important consideration for the compensation mechanism), and elementwise standardisation of the input. These hyperparameters were chosen as standard values, fixed across training to ensure maximal comparability. Standardisation ensures that, elementwise, the samples have zero mean and a standard deviation of 1 across the dataset, unless all samples have an element equal to 0, in which case it remains 0. This approach was used across all experiments, and default train-test data splits were utilised. Cross-entropy loss was used across all classification experiments alongside isotropic-tanh, $\mathbf{f}(\vec{x}) = \tanh(\|\vec{x}\|_2) \hat{x}$, as the activation function in every case. For neurogenesis, the appended scaffold neurons were initialised with outgoing weights as $\vec{W}^* \sim \mathcal{N}(\vec{0}, 0.02 \times \mathbf{I})$, intended to provide a small symmetry-breaking perturbation as needed, while being sufficiently small such that this initial biased direction can be potentially overridden by optimisations. Other approaches to non-zero initialisation could have been explored, such as a linear combination of existing columns, but this was considered to be a stronger inductive bias. The number of independent repeats varied per experiment. All code and seeds used in the production of plots are available at <https://github.com/GeorgeBird1/Isotropic-Adaptive-MLPs>, to enable reproduction. Experiments were conducted on an NVIDIA RTX 3080 10GB GPU with 128 GB of DDR3 RAM.

Architecture, number of epochs and dataset varied by experiment to show a breadth of networks in which the theoretical claims can be verified, and epochs varied due to the individual nature of the experiments.

I.1 Experiment One: Function-Invariance to Neuroadaptation

The objective of this experiment was to verify that adapting the width of a trained network can be undertaken with minimal functional change, owing to the symmetry-led network construction. In particular, this invariance should hold without subsequent retraining following the architectural adaptation. The experiment explored several different approaches for the compensatory parameters of intrinsic length, o , and $\vec{\psi}$.

For this verification experiment, CIFAR-10 classifiers were utilised on an isotropic multilayer perceptron architecture consisting of the structure [3072, 100, 100, 10]. Networks were trained for 50 epochs each, across 20 independent repeats, per configuration. The configurations are as follows:

1. “ $o_{\text{none}}, \vec{\psi}_{\text{decay}}$ ” consists of networks with no intrinsic length parameters, but they do include a trainable psi-vector compensatory parameter, which does have an L_2 decay term such that it tends to the zero vector. The stated algebra is used to transform psi under neuroadaptation.
2. “ $o_{\text{constant}}, \vec{\psi}_{\text{decay}}$ ” consists of networks with a constant, non-trainable, intrinsic length parameter, and they include a trainable psi-vector compensatory parameter, decaying to the zero vector. The stated algebra is used to transform intrinsic length and psi under neuroadaptation.
3. “ $o_{\text{trainable}}, \vec{\psi}_{\text{decay}}$ ” consists of networks with a trainable intrinsic length parameter, and they include a trainable psi-vector compensatory parameter, decaying to the zero vector. The stated algebra is used to transform intrinsic length and psi under neuroadaptation.
4. “ $o_{\text{trainable}}, \vec{\psi}_{\text{none}}$ ” consists of networks with a trainable intrinsic length parameter, and no psi-vector compensatory parameter. The stated algebra is used to transform intrinsic length.

5. “ $o_{\text{trainable}}, \vec{\psi}_{\text{constant}}$ ” consists of networks with a trainable intrinsic length parameter, and they include a constant psi-vector compensatory parameter. The stated algebra is used to transform intrinsic length and psi under neuroadaptation.
6. “ $o_{\text{trainable}}, \vec{\psi}_{\text{trainable}}$ ” consists of networks with a trainable intrinsic length parameter, and they include a trainable psi-vector compensatory parameter, not decaying to zero. The stated algebra is used to transform intrinsic length and psi under neuroadaptation.
7. “ $o_{\text{trainable}}, \vec{b}_{\text{adjusted}}$ ” consists of networks with a trainable intrinsic length parameter, and no psi-vector compensatory parameter. The stated algebra is used to transform intrinsic length, and it uses the $\vec{b}'_2 = \vec{b}_2 + \mathbb{E}[\vec{\sigma}(\cdot)] \vec{W}_* b_*$ to transform the bias vector.

These trained networks then undergo adaptation of their $\mathbb{R}^{100} \rightarrow \mathbb{R}^{100}$ affine map, *in one step* increasing or decreasing the width by the stated quantity, such as +75, yielding a map $\mathbb{R}^{100} \rightarrow \mathbb{R}^{175}$ or -75 yielding a map $\mathbb{R}^{100} \rightarrow \mathbb{R}^{25}$ — no retraining is then undertaken, such that the invariance of the adaption alone can be analysed. The row stating 0 refers to just a layerwise partial diagonalisation, where the map retains the $\mathbb{R}^{100} \rightarrow \mathbb{R}^{100}$ dimensionality but is reparameterised accordingly.

From this, both the before-and-after L_2 -Distances of the final layer activations (prior to softmax) were taken, averaged over all samples in the dataset, and then the final quoted mean and standard deviation were computed repeat-wise. Test-set accuracy was also recorded, as shown in *App. I.5*, but was considered to be redundant and less informative than the tabulated ϵ L_2 distance measurements, which provided greater resolution of the invariance. This is because sufficiently small ϵ results in a negligible change in test-accuracy, which constitutes a discrete samplewise quantity instead of the continuous ϵ stated. Thus, the network was shown to be invariant under neurogenesis, and this invariance was well approximated under neurodegeneration.

Tabulated also in *Tab. 1* are the before (Σ_0) and after (Σ_1) singular value summations, indicating how the neuroadaptation affects the weight parameters. Since the singular values are positive, the sum provides a tabular insight into how neuroadaptation affects the network’s weights.

It was observed that a negligible difference occurred between constant and trainable $\vec{\psi}$ or o in the table. This is because these networks did not undergo retraining, where the constant or trained values would exhibit static or dynamic trajectories. Therefore, the nature of these parameters did not have the opportunity to influence the later invariance, leading to comparable results. Nevertheless, accuracy is reported in *Tab 4*, which displays the accuracy invariance also. The baseline accuracies indicate how the various approaches to psi-vector and intrinsic-length compensatory parameters affected training over the 50 epochs preceding neuroadaptation. They display only a marginal effect, suggesting their role is largely limited to the neuroadaptive compensations for which they were derived, rather than a broader utility as parameters during training.

Table 4: Displays test-set accuracy after neuroadaptation at layer $L = 1$. For the baseline row, values indicate test accuracies prior to adaptation. For all other rows, values are paired within-repeat accuracy changes, $a_{\text{after}} - a_{\text{before}}$. Mean \pm standard deviation is displayed over the 20 repeats.

Neuroadaptation	$o_{\text{none}}, \vec{\psi}_{\text{decay}}$	$o_{\text{constant}}, \vec{\psi}_{\text{decay}}$	$o_{\text{trainable}}, \vec{\psi}_{\text{decay}}$	$o_{\text{trainable}}, \vec{\psi}_{\text{none}}$	$o_{\text{trainable}}, \vec{\psi}_{\text{constant}}$	$o_{\text{trainable}}, \vec{\psi}_{\text{trainable}}$	$o_{\text{trainable}}, \vec{b}_{\text{adjusted}}$
75	+0.001 \pm 0.002	+0.001 \pm 0.002	+0.001 \pm 0.002	-0.001 \pm 0.003	+0.001 \pm 0.003	-0.001 \pm 0.004	-0.000 \pm 0.002
50	+0.001 \pm 0.002	+0.001 \pm 0.002	+0.001 \pm 0.002	-0.001 \pm 0.003	+0.001 \pm 0.003	-0.001 \pm 0.004	-0.000 \pm 0.002
25	+0.001 \pm 0.002	+0.001 \pm 0.002	+0.001 \pm 0.002	-0.001 \pm 0.003	+0.001 \pm 0.003	-0.001 \pm 0.004	-0.000 \pm 0.002
5	+0.001 \pm 0.002	+0.001 \pm 0.002	+0.001 \pm 0.002	-0.001 \pm 0.003	+0.001 \pm 0.003	-0.001 \pm 0.004	-0.000 \pm 0.002
1	+0.001 \pm 0.002	+0.001 \pm 0.002	+0.001 \pm 0.002	-0.001 \pm 0.003	+0.001 \pm 0.003	-0.001 \pm 0.004	-0.000 \pm 0.002
0	+0.001 \pm 0.002	+0.001 \pm 0.002	+0.001 \pm 0.002	-0.001 \pm 0.003	+0.001 \pm 0.003	-0.001 \pm 0.004	-0.000 \pm 0.002
-1	+0.001 \pm 0.002	+0.001 \pm 0.002	+0.001 \pm 0.002	-0.003 \pm 0.010	+0.002 \pm 0.004	-0.001 \pm 0.004	-0.001 \pm 0.006
-5	0.000 \pm 0.019	+0.001 \pm 0.013	+0.002 \pm 0.015	+0.003 \pm 0.050	-0.003 \pm 0.012	-0.002 \pm 0.015	+0.002 \pm 0.023
-25	+0.002 \pm 0.079	-0.014 \pm 0.066	-0.018 \pm 0.064	-0.055 \pm 0.159	0.000 \pm 0.090	-0.028 \pm 0.079	-0.081 \pm 0.078
-50	+0.002 \pm 0.086	-0.019 \pm 0.074	-0.018 \pm 0.058	-0.072 \pm 0.153	+0.001 \pm 0.094	-0.029 \pm 0.090	-0.085 \pm 0.082
-75	-0.009 \pm 0.088	-0.019 \pm 0.084	-0.028 \pm 0.067	-0.097 \pm 0.175	-0.009 \pm 0.108	-0.025 \pm 0.086	-0.098 \pm 0.082
Baseline	44.025 \pm 0.348	44.081 \pm 0.400	44.036 \pm 0.291	44.025 \pm 0.316	44.195 \pm 0.207	43.971 \pm 0.373	44.214 \pm 0.358

Exploring all permutations of approaches to the psi-vector and intrinsic length would have required extensive compute, without yielding further meaningful insight or interpretation. Therefore, comparing intrinsic length approaches against a trainable psi-vector and comparing psi-vector approaches against a trainable intrinsic length provided the most informative combinations for practical implementation of this neuroadaptive methodology.

I.2 Experiment Two: Singular Value and Bias Spectra Evolutions

This experiment displays the evolution of the layerwise singular value and bias spectra of a static isotropic multilayer perceptron over 40 repeats of the architecture [3072, 100, 100, 10], to assess whether the spectra shift during training and whether thresholding the singular values is reasonable. The spectra of bias elements are included for completeness. These networks were trained on CIFAR10 for the displayed 40 epochs, with aforementioned standardisation. The spectrum was pooled across all independent repeats at each epoch snapshot.

As with all experiments, orthogonal initialisation was consistently used to ensure that all initial singular values were equal to 1. Hence, this reduces ambiguity about whether a singular value is increasingly significant to the function or is decaying to become negligible by providing a known initial state of 1. This contrasts with random-normal approaches, which typically have a more distributed spectrum, obfuscating such trends. A slightly boosted learning rate of $\eta = 0.05$ was used to accentuate the long-term trend evolution over the 40 epoch window, enabling more repeats to be taken. This enabled the increase, decay and separation of singular values to be observed more easily, limited to this experiment. This was made possible because final classification accuracy was not important for this particular experiment, but rather a clearer diagnosis of whether singular-value thresholding is experimentally plausible. Together with experiment three, this thresholding was deemed appropriate.

I.2.1 Comparison to Identical Architecture with Standard Tanh

In the plots of *Fig. 2* (and repeated in *Fig. 4*), one can observe a distinct learning-induced spectral shift, particularly in layer zero’s ($\mathbb{R}^{3072} \rightarrow \mathbb{R}^{100}$) singular values and biases — with part of the bulk decaying towards small values while a higher-magnitude tail remains separated. This suggests that training produces amplification along particular directions. A similar pattern is observed for layer two ($\mathbb{R}^{100} \rightarrow \mathbb{R}^{10}$), which exhibits several distinct narrow singular-value modes and biases that emerge during training, with an eventual progressive decay of several bias ridges. Layer one ($\mathbb{R}^{100} \rightarrow \mathbb{R}^{100}$) shows mostly low singular values, with a small band around magnitude 100 and biases around zero. Considered together, isotropic-tanh plots consistently show stronger stratification than in *Fig. 5*, suggesting parameters become highly anisotropic despite the isotropic activation form. The data and task are intrinsically anisotropic due to the image-to-classification objective, and the emergence of anisotropic parameters in isotropic networks indicates a clear, spontaneous symmetry breaking necessitated to achieve this, with a few singular directions becoming specialised while many decay. This contrasts with standard tanh networks, which tend to distribute their spectra as a broad bulk, aligning with more classical interpretations of them as feature detectors.

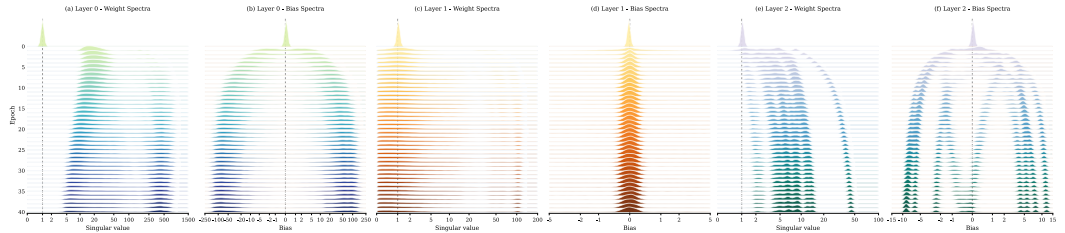


Figure 4: Experiment Two (*App. I.2*) displays the evolving layerwise singular value and bias spectra for a [3072, 100, 100, 10] fixed **isotropic-tanh** MLP trained on CIFAR10 classification. The spectra are obtained from 40 independent repeats, showing strong consistency. Singular values begin at one, indicated by the dashed line, due to orthogonal initialisation, and biases at zero due to initialisation.

The standard-tanh comparison of *Fig. 5* shows a more pronounced and non-decaying spectra in layers zero and one for singular values, showing this largely coherent bulk evolution — which is suggested to contribute to pruning difficulties. The final layer shows little diversification, with training staying peaked around the initialised values with a small decay of some singular values — this suggests it may act largely as a semi-orthogonal transform.

This generally suggests that isotropic-tanh networks tend to have a greater utilisation of the final layer compared to standard-tanh networks, whilst standard-tanh shows a smoother zeroth-layer spectrum,

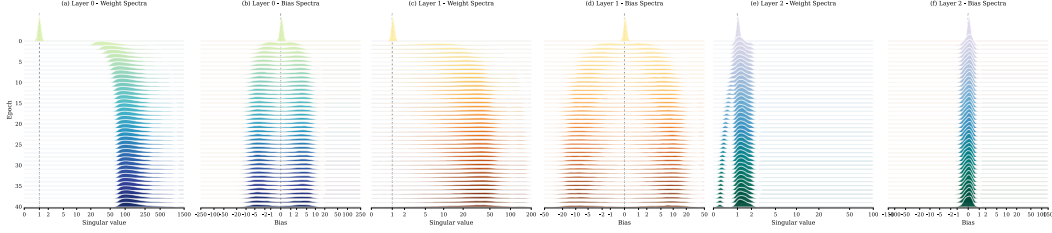


Figure 5: Identical in every way to the results of *Fig. 4* but using a **standard-tanh** instead of isotropic-tanh.

consistent with many directions being amplified to comparable magnitudes. Thus, they appear to exhibit different computational regimes. Isotropic tanh exhibits a distinct, well-separated ordering of its singular values, particularly in the last layer, supporting the paper’s motivation that singular values may be interpreted as having a perturbative impact on the function. The strong similarity across repeats may also be due to the flat-loss orbit induced by the continuous orthogonal equivariance per layer, where many optimisation trajectories may follow comparable paths up to a rotation, because they are not deflected by the loss structure that emerges along those orbits for permutation-derived primitives.

Overall, both demonstrate qualitatively different modes of learning, indicating a lack of true comparability between the forms despite the superficial use of tanh. Caution around classical interpretations of spectra is warranted, as they may be predicated on elementwise activation geometry, thereby limiting their direct reapplication to isotropic networks.

I.3 Experiment Three: Thresholded Neuroadaptation to Changing Task Schedule

This experiment directly tests the threshold-based approach to neuroadaptation by observing how the isotropic multilayer perceptron adapts to a changing task scheduler. Unlike experiment one (*App. I.1*), neuroadaptation occurs after every epoch using the thresholding to automatically adapt three different layers’ widths. This enables the determination of whether this approach adapts as expected to changing task demands while maintaining competitive task performance relative to a non-adaptive control network.

Three distinct image-classification datasets are utilised: MNIST [36], Fashion-MNIST (abbreviated to FMNIST) [37], and the ‘A’ to ‘J’ character samples derived from EMNIST [38]. During training, all samples are provided as input; the scheduler only determines whether each dataset’s cross-entropy term contributes to the overall loss, which the network is optimised against. Hence, the architecture is described by the structure [2352, H1, H2, H3, 30], where H1, H2, H3 are initialised uniformly: $H1, H2, H3 \sim U(0, 2500)$. This was determined to be a reasonable range, producing adaptations for both initial under- and overabundance of neurons. It was noted that when there were fewer than ≈ 500 initial neurons, the growth permitted by the $\Xi = 5$ scaffold neurons was often insufficient to meet demand, repeatedly triggering neurogenesis with too little time to grow before the next schedule. The singular value thresholding was chosen at $\vartheta = 0.95$ to quickly neurodegenerate unused parameters, decaying immediately from an initial value of 1 due to the orthogonal initialisers. Using this, 5 ‘scaffold’ neurons are maintained as a buffer below this threshold. The 30-width output corresponds to three disjoint ten-class label blocks, over which softmax is separately applied. This structure permits the scheduler to activate a task via a Boolean switch, S_{dataset} , and the total loss is averaged to reduce discontinuity upon task-switching, as shown by *Eqn. 54*.

$$\mathcal{L}_{\text{total}} = \frac{S_{\text{MNIST}}\mathcal{L}_{\text{MNIST}} + S_{\text{FMNIST}}\mathcal{L}_{\text{FMNIST}} + S_{\text{EMNIST}}\mathcal{L}_{\text{EMNIST}}}{S_{\text{MNIST}} + S_{\text{FMNIST}} + S_{\text{EMNIST}}} \quad (54)$$

Using this setup, 25 independent repeats were taken to produce *Fig. 3* with a schedule described by *Tab. 5*. Accuracies were still gathered for all datasets, regardless of whether the corresponding loss contributed to the total loss. A static model with identical initialisation was used as a control across all repeats and allowed the stated adaptive-versus-control accuracies to be determined at the T3 schedule boundary.

Table 5: Task schedule used in Experiment Three.

Epoch range	Active dataset(s)
0–149	MNIST
150–299	MNIST + Fashion-MNIST
300–449	MNIST + Fashion-MNIST + EMNIST A–J
450–599	Fashion-MNIST

I.4 Experiment Four: Initial Under-to-Over Neuron Abundance

The objective of this experiment was to determine the benefit of initial neuron under- or over-abundance on test accuracy. It achieved this by training the starting networks for 15 epochs at the initial width, then undergoing gradual (at a linear rate) neuroadaptation for 75 epochs to the desired width, followed by a final 10 epochs post-training at the final width. This was undertaken for four repeats per permutation, with all permutations of $n = \{7, 10, 25, 50, 75, 100\}$ starting and ending widths trialled for a CIFAR-10 classification network of architecture [3072, $n, n, 10$]. This totals 144 independent networks trained for this experiment. The $n = 7$ permutations were added to investigate insufficient-width networks for CIFAR10.

Overall, this experiment was less revealing, showing no statistically significant trend other than dependence on final width; however, this is suggestive that the neuroadaptive methodology was successful in preserving function path-independently, since similar or higher performance was achieved for dynamic networks than for the fixed-width controls. Several of the highest recorded accuracies were obtained with a small starting width of 7 or 10, but the error reduces the significance of these results.

I.5 Experiment Five: Sparsification

In *Sec. 2.2.1*, a reduction in the number of parameters is detailed using the full-diagonalisation approach, whilst retaining all prior functions. This section verifies these theoretical claims, demonstrating that a substantial reduction in parameters can be achieved with negligible function detriment. The derived formulae demonstrated that the reduction can asymptotically achieve 50% sparsity at infinite width and depth, whilst this section empirically details various finite-width and depth architectures and the respective practical sparsification fractions achieved.

To ensure initial functionality, these networks were trained with the above hyperparameters stated at the beginning of *App. I*, on CIFAR-10 classification for 25 epochs over 5 independent repeats. Results of *Tab. 6* shows mean and standard deviation statistics for a range of network architectures.

It is also important to clarify that *Sec. 2.2.1*'s *Eqns. 14* and *15*, count the weight and bias parameters. Introduced later are the intrinsic length and $\bar{\psi}$ compensatory parameters, which the networks below utilise. Hence, a slight modification to account for these additional parameters is detailed in *Eqn. 55* for odd-length networks, and *Eqn. 56* for even-length networks. These additional parameters contribute $+N + 1$ parameters per layer, which cannot be diagonalised and therefore persist in the numerator and denominator. These do not affect the stated asymptotic results and apply to constant-width networks.

$$S_{\text{odd}} = \frac{D(3N + 1) + (D + 1)(N^2 + 2N + 1)}{(2D + 1)(N^2 + 2N + 1)} = \frac{1 + D^{-1}}{2 + D^{-1}} + \frac{D(3N + 1)}{(2D + 1)(N + 1)^2} \quad (55)$$

$$S_{\text{even}} = \frac{(D - 1)(3N + 1) + (D + 1)(N^2 + 2N + 1)}{2D(N^2 + 2N + 1)} = \frac{1 + D^{-1}}{2} + \frac{(D - 1)(3N + 1)}{2D(N + 1)^2} \quad (56)$$

The results of *Tab. 6* verify finite-width sparsity with function invariance, demonstrating negligible change in the final-layer output activations, with L_2 -distances around $\epsilon \approx 10^{-3}$ and a $\approx 10^{-3}\%$ change in classification accuracy, whilst achieving a 13% to 37% parameter reduction. The alternating diagonalised architecture is also computationally more efficient in the forward pass, as the

Table 6: Post-training sparsification of CIFAR-10 classifiers. Architectures notated compactly as $w \times k$ for the k hidden layers of width w . Change in per-repeat accuracy denoted as Δ_{acc} . Parameter counts are non-zero parameters, reported in millions, using the threshold $|\theta| > 10^{-4}$. Discrepancy ϵ is the mean test-set activation L_2 -distance between the original and sparsified networks.

Architecture	Acc. before	Δ acc. ($\times 10^{-2}$ pp)	Params before	Params after	% Reduced	ϵ ($\times 10^{-4}$)
[3072, 500×2, 10]	43.2±0.4	+0.0±0.0	1.79M	1.54M	14.0%	4.7±2.0
[3072, 500×3, 10]	45.0±0.5	-0.4±1.1	2.04M	1.79M	12.3%	15.5±1.4
[3072, 500×4, 10]	45.5±0.2	-0.6±0.9	2.29M	1.79M	21.8%	14.4±2.4
[3072, 500×5, 10]	45.2±0.2	+0.4±1.1	2.54M	2.04M	19.7%	9.4±1.7
[3072, 500×6, 10]	43.2±0.7	+0.0±0.0	2.79M	2.04M	26.9%	11.5±2.6
[3072, 1000×2, 10]	43.2±0.4	-0.2±0.4	4.08M	3.08M	24.6%	7.5±1.5
[3072, 1000×3, 10]	44.8±0.6	-0.4±1.1	5.08M	4.08M	19.7%	24.8±4.6
[3072, 1000×4, 10]	45.2±0.3	-0.0±1.2	6.08M	4.08M	32.9%	18.7±3.4
[3072, 1000×5, 10]	44.0±0.9	-0.4±1.1	7.08M	5.08M	28.3%	18.7±8.4
[3072, 1000×6, 10]	41.5±1.1	-0.4±0.5	8.08M	5.08M	37.1%	13.5±3.5

diagonalisation yields a Hadamard product rather than full matrix multiplication. Thus, this technique may be used prior to inference to obtain a more computationally and parameter-efficient isotropic multilayer perceptron architecture.

I.6 Experiment Six: Isotropic-Tanh Against Standard-Tanh Trends

Already established in the previous discussion is that standard-tanh, $\mathbf{f}(\vec{x}; \{\hat{e}_i\}) = \sum_i \tanh(\hat{e}_i^T \vec{x}) \hat{e}_i$, does not operate comparably to isotropic-tanh, $\mathbf{f}(\vec{x}) = \tanh(\|\vec{x}\|_2) \hat{x}$, despite their superficial resemblance and function agreement for vectors colinear with basis directions, \hat{e}_i . Nevertheless, comparison can be undertaken across various datasets, but one should not assess either’s broader functional form on a single instance alone. The results consist of four repeats for each network-activation function permutation, across datasets of arguably increasing difficulty: MNIST, A-J EMNIST, Fashion-MNIST, CIFAR10, CIFAR100 and Caltech-256 [56] — each trained for 50 epochs. Caltech-256 was resized to 64×64 pixels per sample. The architecture column specifies the hidden layer width W and the number of hidden layers D ($W \times D$), with the input and output dimensions constrained by their respective datasets.

Table 7: Experiment Six: displays the final test-set accuracy for standard-tanh and isotropic-tanh for otherwise identical multilayer perceptrons across various datasets and architectures. Values are reported as mean \pm standard error. Boxed indicates column-wise highest accuracy, bold indicates pairwise highest accuracy.

Architecture	MNIST		EMNIST-AJ		FMNIST		CIFAR-10		CIFAR-100		CALTECH-256	
	Standard	Isotropic	Standard	Isotropic	Standard	Isotropic	Standard	Isotropic	Standard	Isotropic	Standard	Isotropic
500×2	97.18±0.03	94.38±0.04	93.26±0.09	86.69±0.20	87.58±0.23	85.69±0.14	44.70±0.11	44.16±0.09	18.70±0.07	18.60±0.11	14.22±0.19	12.88±0.16
500×3	97.07±0.04	95.28±0.11	93.24±0.02	87.81±0.18	87.77±0.09	86.13±0.16	45.19±0.13	45.36±0.21	18.62±0.15	19.62±0.10	13.45±0.16	13.63±0.12
500×4	96.83±0.08	95.25±0.09	93.26±0.05	88.32±0.06	86.96±0.13	86.04±0.25	44.83±0.18	45.92±0.16	17.23±0.15	18.91±0.10	12.63±0.21	12.82±0.15
500×5	96.61±0.08	95.37±0.07	93.27±0.09	89.80±0.20	86.66±0.30	85.77±0.32	43.49±0.28	45.95±0.34	15.97±0.09	17.22±0.05	11.66±0.38	12.41±0.09
1000×2	96.98±0.05	94.33±0.06	93.15±0.02	86.62±0.17	86.66±0.27	85.62±0.15	42.18±0.34	44.19±0.08	17.74±0.06	18.68±0.10	12.71±0.12	12.93±0.05
1000×3	96.77±0.07	95.33±0.09	93.04±0.20	88.19±0.10	86.72±0.16	86.02±0.13	42.76±0.24	45.45±0.22	16.68±0.10	19.59±0.10	12.44±0.22	13.54±0.09
1000×4	96.74±0.04	95.32±0.18	92.61±0.16	88.49±0.05	86.08±0.18	85.97±0.28	41.97±0.39	46.02±0.12	14.45±0.19	18.73±0.11	10.57±0.18	13.07±0.07
1000×5	96.60±0.13	95.15±0.12	92.22±0.03	89.69±0.11	85.60±0.12	85.98±0.22	39.56±0.25	45.58±0.57	12.31±0.21	17.02±0.15	8.40±0.53	12.37±0.10

The trend appears quite stable, showing a preference towards isotropic-tanh for more conventionally challenging image classification datasets, particularly for deeper MLPs — with the converse for standard-tanh. This does demonstrate that their optimal regimes are dataset and architecture-dependent; however, isotropic-tanh is a more encouraging result for broader application, demonstrating preferable scalability with challenging datasets and deeper architectures. CIFAR and CALTECH results demonstrate a considerable advantage typically for isotropic-tanh, whilst MNIST and EMNIST-AJ show an advantage of standard-tanh, with a narrower performance gap for Fashion-MNIST.

Further tendencies are observed: standard-tanh seems to decline considerably with increasing depth or width, a phenomenon much more suppressed in the isotropic formulation’s results. This suggests that the isotropic-tanh may alleviate depth-related pathologies present in standard-tanh networks.

Overall, this is a promising tendency for isotropic-tanh; it is superior for deeper-wider networks, whilst standard-tanh’s regime is confined to narrower-shallower networks. This reliable superiority

of isotropic tanh across these harder datasets and larger architectures regimes does alleviate some concerns raised in *App. G* regarding expressibility of isotropic functions; however, this must be considered only a single instance of tanh and not yet expanded more broadly. This remains encouraging, considering that the standard tanh was a popular choice historically, before the advent of more modern activation functions. Thus, development from isotropic-tanh's foundation may be undertaken to a similar effect, via a naive search over function space or theoretical developments.